# Nonclassical Cold-Frontal Structure Caused by Dry Subcloud Air in Northern Utah during the Intermountain Precipitation Experiment (IPEX)

DAVID M. SCHULTZ

*Cooperative Institute for Mesoscale Meteorological Studies, University of Oklahoma, and NOAA/National Severe Storms Laboratory, Norman, Oklahoma*

ROBERT J. TRAPP

*Department of Earth and Atmospheric Sciences, Purdue University, West Lafayette, Indiana*

(Manuscript received 11 November 2002, in final form 11 April 2003)

ABSTRACT

The purpose of the Intermountain Precipitation Experiment (IPEX) is to improve understanding of precipitating systems in the Intermountain West. Instrumentation deployed during the field phase of IPEX sampled a strong cold front and associated convection that moved through northern Utah on 14–15 February 2000. The surface cold front was characterized by a sharp temperature drop (8°C in 8 min), strong pressure rise (3 hPa in 30 min), and gusts to 40 m $s^{-1}$. The temperature drop at high-elevation surface stations (2500–3000 m MSL) preceded the temperature drop at low-elevation surface stations (1290–2000 m MSL) by as much as an hour, implying a forward- or downshear-tilting frontal structure. Consistent with the cooling aloft, a hydrostatic pressure rise and wind shift preceded the temperature drop at the surface. Radar captured the rapid evolution of the wind shift line into a gravity current. A forward-sloping cloud with mammatus and a 20-hPa-deep superadiabatic layer underneath were observed by radar and radiosondes, respectively. Shading from this forward-sloping cloud is believed to have produced a surface-based prefrontal inversion upon which a solitary gravity wave traveled. These and other observations reveal that the forward-sloping cloud generated by a shortwave trough aloft was producing precipitation that sublimated, melted, and evaporated in the dry subcloud air (dewpoint depression of 5°–10°C), causing the cooling aloft and the nonclassical frontal structure.

Although the storm-total precipitation associated with this system was generally light (less than 20 mm at all observing sites), the amount of precipitation was strongly a function of elevation. During one 6-h period, precipitation at stations above cloud base (roughly 2000 m MSL) varied widely, mostly due to orographic effects, although precipitation amounts at most stations were about 7–11 mm. In contrast, precipitation amounts decreased with distance below cloud base, consistent with sublimation and evaporation in the dry subcloud air.

## 1. Introduction

Damaging winds occurred throughout northern Utah on 14–15 February 2000. (Figure 1 is a map of observing stations and geographic locations.) Twenty-five thousand Salt Lake County residents were left without power for 2 h (NCDC 2000, p. 108) by large-scale southerly winds gusting over 26 m $s^{-1}$ (Fig. 2). Following the southerlies, winds associated with a strong surface cold front and convective line produced southwesterly, westerly, and northwesterly gusts as high as 40 m $s^{-1}$ (Fig. 2). The winds toppled an 80-year-old tree onto a car and killed the owner, a 38-year-old woman, as she walked to her house in Brigham City, Utah (NCDC 2000, p. 108; Fig. 2). Northwesterly winds behind the front overturned the shallow waters of Farmington Bay in the Great Salt Lake releasing odor from decaying organic material and generating ''lake stink,'' affecting the downwind populated areas. At its most intense, the front was moving 26 m $s^{-1}$ and was associated with a temperature decrease of 8°C in 8 min and a pressure rise of 3 hPa in 30 min. Surprisingly, within 150 km and 3 h, the front slowed to half its previous speed and weakened, yielding a local temperature decrease of only 1°C within 15 min. The convection and severe weather abruptly ended, and the remaining precipitation evolved into showers. By storm's end, snowfall in the Wasatch Mountains included 5 cm (2 inches) in the town of Park City, 23 cm (9 inches) at Alta, and 51 cm (20 inches) at The Canyons Resort (Fig. 2).

This event occurred during the field phase of the Intermountain Precipitation Experiment (IPEX; Schultz et al. 2002), a research program designed to improve the quantitative prediction of precipitation over the Intermountain West of the United States. Known as the Val-

*Corresponding author address:* Dr. David M. Schultz, NOAA/National Severe Storms Laboratory, 1313 Halley Circle, Norman, OK 73069.
E-mail: david.schultz@noaa.gov

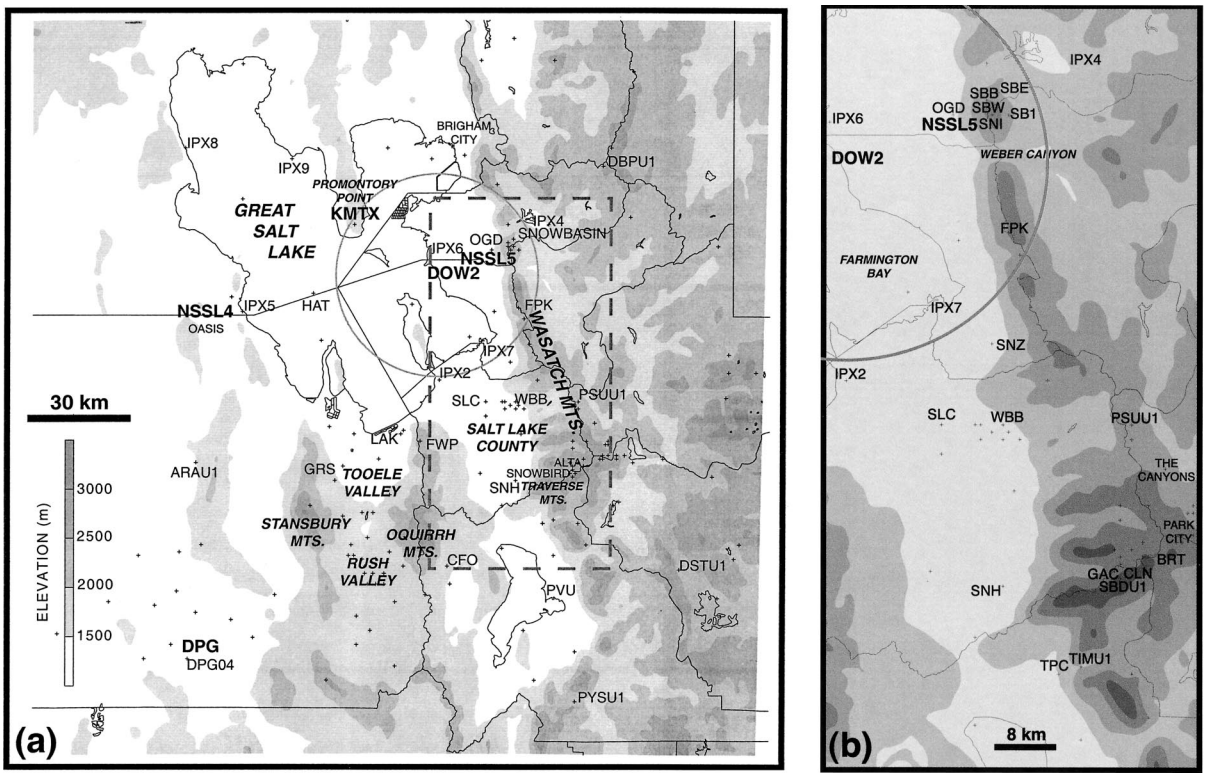


FIG. 1. Geographic and observing-station locations mentioned in the text. Elevation (m) is shaded according to scale. Plus signs indicate locations of available MesoWest stations. Bold roman text labels the special observing systems (e.g., mobile laboratories, radars). Regular roman text labels observing stations, ski resorts, and cities. Bold italic text labels geographic and political areas. Thin solid lines represent county and lake boundaries. The gray circle around DOW2 represents 30-km range ring. (a) Northern Utah: the dashed line represents the location of (b) the detail along the Wasatch Mountains.

entine's Day windstorm, this front was the focus of IPEX's fourth intensive observing period (IOP 4). LaDue (2002) has described the evolution of a tornadic bow echo during this event in the Snake River Valley of southern Idaho.

In this paper, however, we focus primarily on the frontal passage in northern Utah, analyzing data from the IPEX observing facilities (Schultz et al. 2002). These facilities provided high temporal and spatial measurements during the frontal passage, which allow us to address previously undocumented aspects of a front in the Intermountain West. For example, the cooling associated with the front arrived aloft before that at the surface, thus the front appeared to be forward tilting. Hydrostatically, this forward-tilting frontal structure caused the pressure trough associated with the front to occur ahead of the temperature gradient defining the front at the surface. Such a structure implies that this front did not conform to traditional models of rearward-tilting fronts, such as those summarized in review articles (e.g., Keyser 1986; Browning 1990). Although only one example, IPEX IOP 4 bears similarity to other strong cold-frontal passages in the Intermountain West, likely providing some generality to these results.

This paper begins by examining the prefrontal environment and early evolution of the front over Nevada (section 2). In section 3, the microscale aspects of the frontal structure and evolution are explored using surface and upper-air data collected during IPEX. In section 4, data from a Doppler on Wheels (DOW) radar illustrate the structure and the evolution of the front further, particularly that of the leading edge of the front. The spatial distribution of the precipitation in northern Utah, with emphasis on its distribution with elevation, is discussed in section 5. Section 6 reviews the role of subcloud diabatic cooling in creating the observed nonclassical frontal structures and section 7 presents a conceptual model of this event, concluding this paper.

## 2. Development over Nevada

The development, maintenance, and movement of this front throughout the Intermountain West is the subject of a future article. Nevertheless, in this section, we provide a brief overview of the early evolution of the front before it reaches the principal IPEX observing area in northern Utah. The surface cold front intensified from a temperature decrease of 1°C in 9 h along the Pacific Coast to temperature drops as large as 8°C in 1 h over eastern Oregon and western Nevada by around 1800

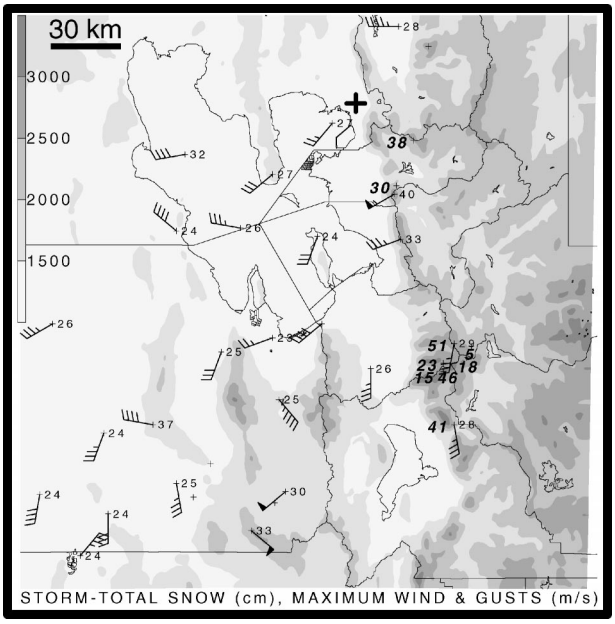


FIG. 2. Wind direction and speed of the strongest winds occurring from 2100 UTC 14 Feb to 0515 UTC 15 Feb 2000 at each station (one pennant, full barb, and half-barb denote 25, 5, 2.5 m $s^{-1}$, respectively), elevation (m, shaded according to scale), maximum wind gusts (m $s^{-1}$, number to right of wind barb), and storm-total snowfall amounts (cm, bold italic numbers). The death described in the text is indicated by a plus sign. Thin solid lines represent county and lake boundaries.

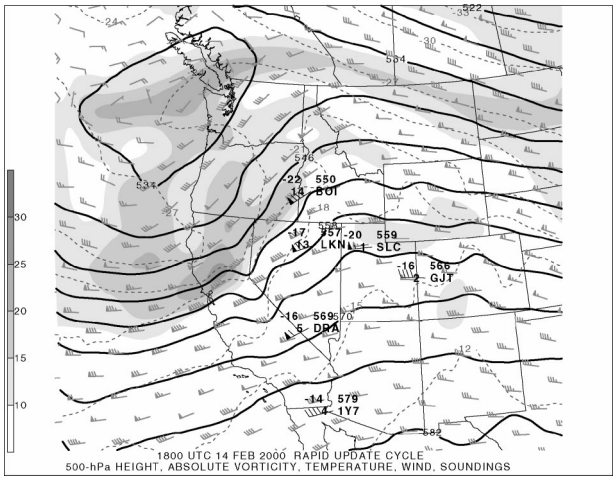


FIG. 3. 1800 UTC 14 Feb 2000: 500-hPa geopotential height (solid lines every 6 dam), absolute vorticity of the total wind ($10^{-5}$ $s^{-1}$, shaded according to scale), temperature (dashed lines every 3°C), and horizontal wind (light gray; one pennant, full barb, and half-barb denote 25, 5, 2.5 m $s^{-1}$, respectively) from the 1800 UTC 14 Feb initialization of the Rapid Update Cycle (Benjamin et al. 1998). Station models with observed sounding data are overlaid: temperature (°C) in upper-left position relative to wind barb, dewpoint depression (°C) to left of wind barb, geopotential height (dam) in upper-right position of wind barb, and station abbreviation to right of wind barb. BOI = Boise, ID; SLC = Salt Lake City, UT; LKN = Elko, NV; GJT = Grand Junction, CO; DRA = Desert Rock, NV; 1Y7 = Yuma Proving Ground, AZ.

UTC 14 February (hereafter 14/1800, not shown). The approach of a 500-hPa absolute vorticity maximum (and cooling) in the mid- and upper troposphere (Fig. 3) was producing ascent as seen on the satellite imagery (not shown). Thus, the cooling between 600 and 300 hPa [as much as 3°–6°C between 14/1106 and 14/2004 over Elko, Nevada (LKN)] and warming below 600 hPa due to both surface heating and advection (as much as 4°–9°C over the same period) was leading to steepening lapse rates and destabilization (Fig. 4a), also observed downstream at SLC (Fig. 4b). In addition, drier air in the lower to midtroposphere was advected into the Intermountain West, producing 5°–10°C dewpoint depressions by 14/2004 at LKN and 14/2313 at SLC (Fig. 4). Although convective available potential energy (CAPE) at LKN was increasing, it was still very small, rising from 0 to 16 J $kg^{-1}$ between 14/1106 and 14/2004. [Throughout this paper, CAPE was computed using a mean-mixed parcel from the surface to 500 m AGL using the virtual temperature correction of Doswell and Rasmussen (1994).] In contrast, the prefrontal wind shear was strong and increasing substantially: the 0–5 km AGL shear increased from 24 m $s^{-1}$ at 14/1430 (the wind profile at 14/1106 was incomplete) to 37 m $s^{-1}$ at 14/2004. Such a low-CAPE–high-shear environment supported the potential for organized severe weather (e.g., Johns et al. 1993; Moller 2001; Hanstrum et al. 2002), confirmed by the strong wind gusts observed throughout Nevada and northern Utah (NCDC 2000). Convection developed in this weakly unstable environment, moved quickly across Nevada, and arrived in northern Utah at 14/2230 with a speed of 26 m $s^{-1}$. The next section of this paper presents more detail on the kinematic and thermodynamic structure of the front as it moved through northern Utah.

## 3. Frontal passage in northern Utah

Radar reflectivity from the WSR-88D radar on Promontory Point (KMTX) at 14/2305 showed a broad line of moderate (up to 35 dBZ) radar echoes (Fig. 5a). The northern portion of the line intensified as it approached the northwestern shore of the Great Salt Lake around 15/0005 (Fig. 5b). After crossing the lake, the strong winds with the accelerating northern portion of the line were responsible for the woman's death in Brigham City at 15/0045 (NCDC 2000, p. 108; Fig. 2). By 15/0100, the southern portion of the line developed a more east-northeast–west-southwest orientation (Fig. 5c). The line began to decelerate after 15/0200 (cf. Figs. 5c,d) and radar echoes along the line began to move parallel to the line (not shown), likely because the line became oriented more parallel to the flow in the mid- and upper troposphere (e.g., the 14/2313 SLC sounding in Fig. 4b).

### *a. MesoWest stations*

As has been noted for a different front by Steenburgh and Blazek (2001, section 3), the location and intensity

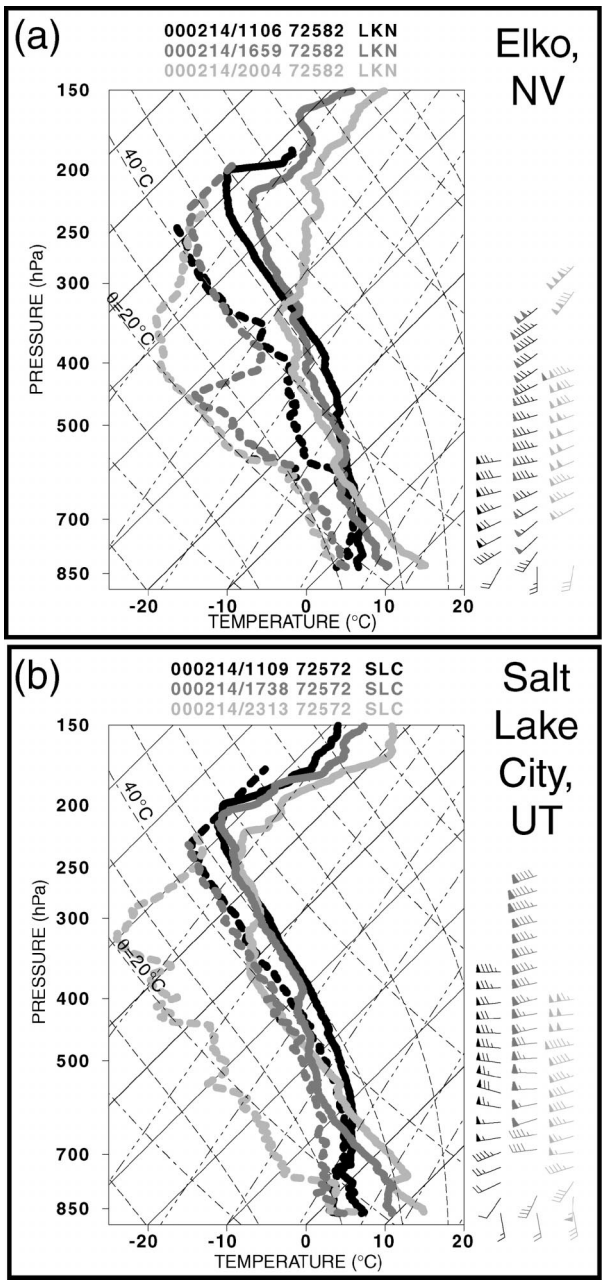


FIG. 4. (a) Skew *T*–log*p* plot of the observed soundings at Elko, NV, released at 1106 UTC 14 Feb (black), 1659 UTC 14 Feb (dark gray), and 2004 UTC 14 Feb 2000 (light gray). Temperature (°C, solid lines), dewpoint temperature (°C, dashed lines), and wind (one pennant, full barb, and half-barb denote 25, 5, 2.5 m $s^{-1}$, respectively). (b) Same as (a) except for Salt Lake City at 1109 UTC 14 Feb (black), 1738 UTC 14 Feb (dark gray), and 2313 UTC 14 Feb 2000 (light gray). The data is 6-s sampling-interval format and is processed using a methodology similar to that of Williams et al. (1993).

of this front can be more precisely determined given the abundant surface stations in northern Utah comprising the MesoWest cooperative networks (Horel et al. 2002). Figure 6 shows the time and magnitude of the initial drop in temperature of 2°F (1.1°C) or greater in 15 min. [We term this decrease in temperature *the front*, in agreement with Bjerknes (1919), Sanders and Doswell (1995), and Sanders (1999a), who emphasized the primacy of temperature (or potential temperature) in surface analysis, even for shallow baroclinic zones associated with diabatic processes.] The front steadily progressed from northwest to southeast, although it moved rapidly eastward over the Great Salt Lake [possibly due to reduced postfrontal boundary-layer turbulence, as discussed, e.g., by Gallus and Segal (1999)]. The front slowed as it approached the northern Wasatch Mountains and the Traverse Mountains [possibly due to (i) blocking of the low-level flow ahead of the front by the mountains, as discussed by Zehnder and Bannon (1988), Braun et al. (1999), and Colle et al. (2002), among others; (ii) weak upper-level forcing (Schumacher et al. 1996; Dickinson and Knight 1999); or (iii) both], followed by an acceleration in the lee of the Wasatch between 0200 and 0300 UTC. The magnitude of the initial temperature drop generally decreased from values as high as 8.3°C in 15 min at Oasis to 1.1°C in 15 min at stations in Tooele Valley, Rush Valley, and the southern Wasatch Mountains (Fig. 6).

Time series from five low-elevation stations (Fig. 7), ranging from Hogup (IPX8) in the northwest to Provo (PVU) in the southeast, showed the decreasing sharpness of the temperature drops as the front moved southeast in time, but comparable total temperature changes from maxima to minima (ranging from 7.2° to 9.3°C), even as the front weakened. [Southern Causeway (IPX2; Fig. 7b) experienced the largest total temperature drop of 10.6°C, but this was enhanced by downslope flow off the Oquirrh Mountains from 14/2255 to 14/0110, producing one of the highest surface temperatures ahead of the front, 16.7°C.] The front can be followed about as far south as Payson Ranger Station (PYSU1) at 15/0500, then a lack of stations and a weak signature in the surface temperature inhibit further tracking of the feature southward (Fig. 6). Following the drop in temperature, nearly all low-elevation (1290–2000 m MSL) stations show a temperature rise following the front (Fig. 7), a feature to be discussed more later in the paper.

To consider the cooling behind the cold front from another perspective, an air parcel from 618 hPa in the 14/2313 SLC sounding (Fig. 4b) possessed 542 J $kg^{-1}$ of downdraft convective available potential energy (DCAPE) (Emanuel 1994; Gilmore and Wicker 1998). Specifically, if evaporation or sublimation of precipitation were sufficient to saturate downdraft air, then the most negatively buoyant air parcel in this sounding would originate at 618 hPa and descend along the 285 K wet-bulb potential temperature ($\theta_w$) pseudoadiabat to the surface, arriving with a temperature of 6°C. Mixing of this air during descent would produce a value of $\theta_w$ warmer than 285 K (e.g., Gilmore and Wicker 1998). If saturated, much of the lower and midtroposphere in the 14/2313 SLC sounding would become negatively

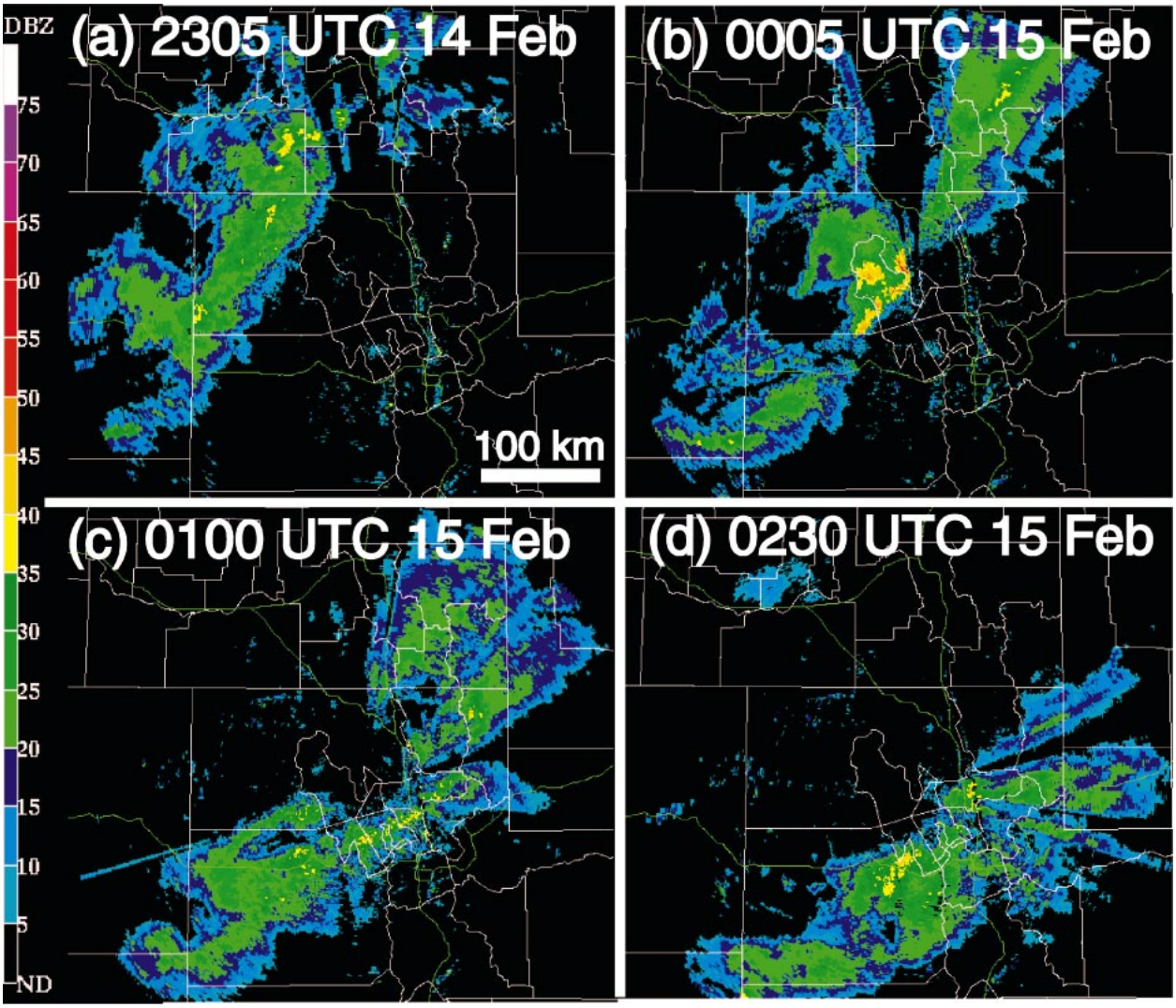


FIG. 5. Base radar reflectivity factor (dBZ, colored according to scale) from the lowest elevation angle (0.5°) of the WSR-88D at Promontory Point, UT (KMTX): (a) 2305 UTC 14 Feb, (b) 0005 UTC 15 Feb, (c) 0100 UTC 15 Feb, and (d) 0230 UTC 15 Feb.

buoyant with respect to the initial sounding. To explore this hypothesis, we examine time series at stations across northern Utah for the simultaneous relative minimum temperature and relative maximum dewpoint temperature behind the front. These temperatures as a function of height follow a moist adiabat and are within a few degrees of 285 K (Fig. 8). Stations above 1700 m are more likely to be saturated (circle within triangle in Fig. 8) with $\theta_w = 283$ K. Thus, the postfrontal surface air was primarily undiluted downdraft air from the lower and midtroposphere.

Despite the intensity of this surface front, the largest temperature drop and minimum in surface pressure were not coincident. Time series from five representative stations (Fig. 9) showed that the pressure minimum preceded the temperature drop by as little as 15 minutes at Hat Island (HAT) to as much as 2 h at Sandy (SNH). (Because most MesoWest stations do not record any form of pressure data, different stations are shown in Fig. 9 than Fig. 7.) Thus, the separation between the pressure trough (hereafter, termed *the prefrontal trough*) and the temperature gradient increased as the front moved southward.

Following the prefrontal trough, the pressure rose sharply, usually in tandem with, but slightly ahead of, the strong drop in temperature (Fig. 9). Winds shifted to the north or northwest and wind speeds increased or decreased, depending on location. The postfrontal winds, however, were usually much less than that required to advance the front by horizontal advection. Therefore, another process to explain the movement of the front is required, which is discussed later.

Within about 1–2 h, the pressure reached a maximum and then remained constant or decreased slightly (Fig. 9), with a return to southerlies bringing warmer, drier air. The wind and the pressure responded to the warmer,

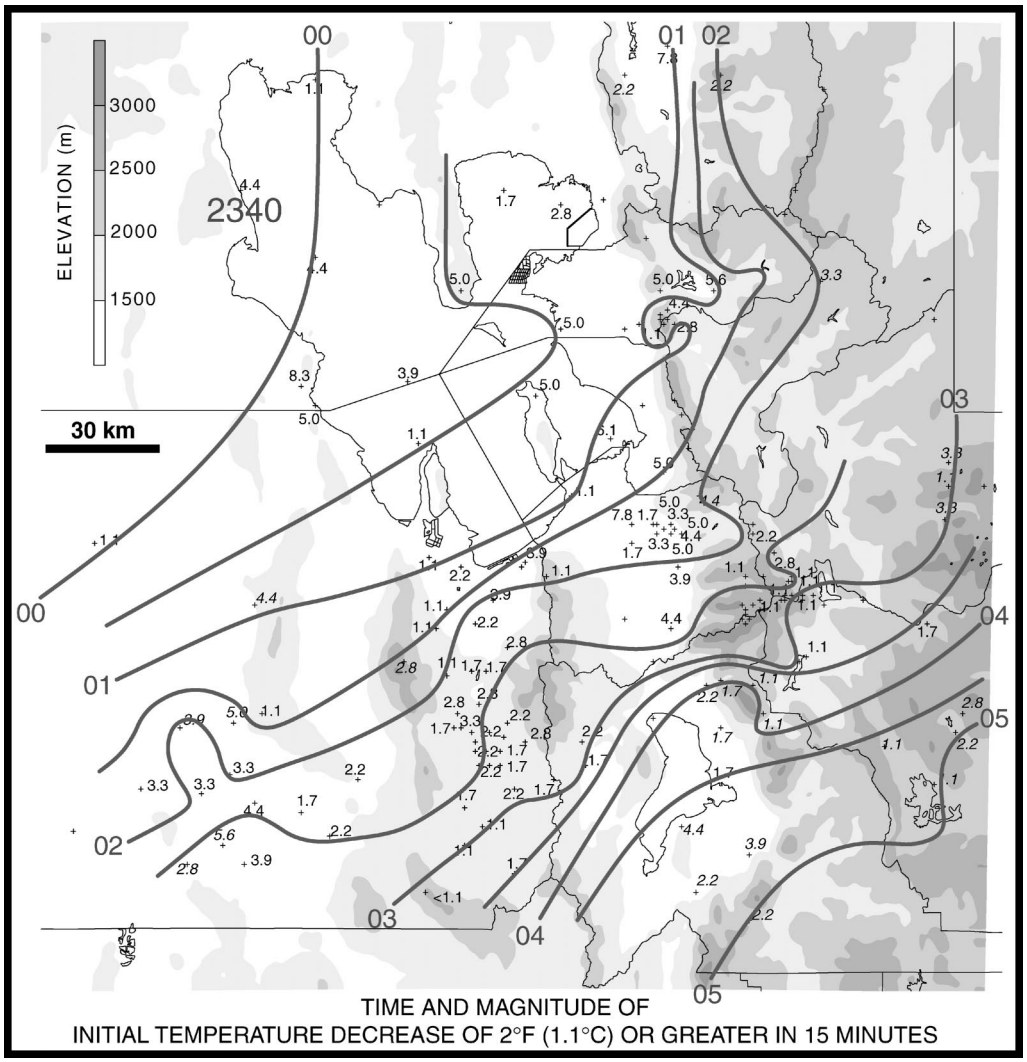


FIG. 6. Isochrones of the front on 15 Feb 2000 as defined by the first drop of 2°F (1.1°C) or greater in 15 min (thick solid lines every 30 min, labeled on the hour). 2340 represents frontal passage at 2340 UTC 14 Feb at that location. Small roman numbers next to plus signs represent magnitude of initial temperature drop in 15 min associated with the front (°C). Small italicized numbers represent temperature drops in 30 or 60 min (°C) for stations that do not report every 15 min.

drier air in a manner similar to that of the divergent outflow at the surface associated with a lower-tropospheric mesohigh (e.g., Fujita 1959), followed by a lower-tropospheric wake low associated with a rear-inflow jet, as in conceptual models of squall lines. [See the review in Johnson (2001) for more about the pressure patterns associated with convective lines.] Why these observations behave in this manner is developed further throughout this paper.

### *b. Surface data from NSSL4 and the SLC ASOS*

A more detailed look at the frontal passage is afforded by two surface observing stations that recorded data very frequently. The first is the National Severe Storms Laboratory (NSSL) mobile laboratory NSSL4 (Rust et al. 1990), which recorded surface weather observations every 6 s. During IOP 4, NSSL4 was located at Oasis on the Utah Test and Training Range, west of the Great Salt Lake. The second is the Automated Surface Observing System (ASOS) from SLC, which recorded data every 1 min.

During the frontal passage, the temperature at NSSL4 fell from 13.9°C at 15/0001:27 to 6.1°C at 15/0009:45, nearly 8°C in 8 min (Fig. 10a). Similar measurements were obtained at SLC, where the temperature dropped from 14.4°C at 14/1829 to 6.7°C at 14/1837 (Fig. 11a). Since the front was moving at 26 m $s^{-1}$, this was consistent with a horizontal temperature gradient of 6.0°C $(100\ m)^{-1}$.

As at the stations presented in Fig. 9, the surface pressure at NSSL4 and SLC reached a minimum about

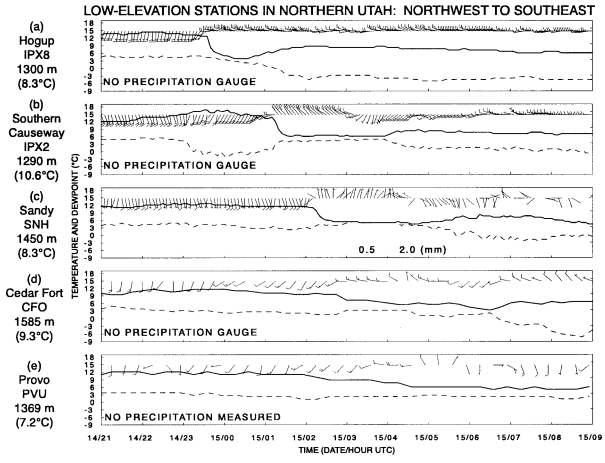


FIG. 7. Time series from (a) Hogup (IPX8, elevation 1300 m MSL), (b) Southern Causeway (IPX2, 1290 m), (c) Sandy (SNH, 1450 m), (d) Cedar Fort (CFO, 1585 m), and (e) Provo (PVU, 1369 m). Temperature (°C, solid lines), dewpoint temperature (°C, dashed lines), 1-h precipitation amount (mm, numbers along bottom, unless otherwise noted), and wind (one pennant, full barb, and half-barb denote 25, 5, and 2.5 m $s^{-1}$, respectively). The total temperature change (number in parentheses under the station elevation) is defined as the difference between the prefrontal maximum temperature and postfrontal minimum temperature between 14/2100 and 15/0900.

an hour (93 km) prior to the largest temperature drop (Figs. 10a and 11a,b). At NSSL4, the wind began to shift from south-southeast to west ahead of the temperature drop in concert with the prefrontal pressure rise (Fig. 10b). The majority of the wind shift (90° of the total 110°) occurred before the temperature started dropping. By the time of the largest temperature decrease,

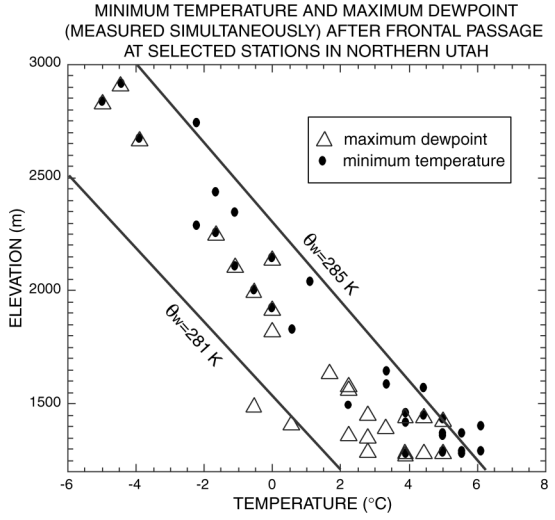


FIG. 8. Postfrontal relative minima in temperature (°C, solid circles) and relative maxima in dewpoint temperature (°C, open triangles) vs elevation (m) for selected stations in northern Utah that experience recovering temperatures after frontal passage. Minimum temperatures and maximum dewpoints were recorded simultaneously at each station between 14/2100 and 15/0900. Approximate $\theta_w$ pseudoadiabats in gray lines.

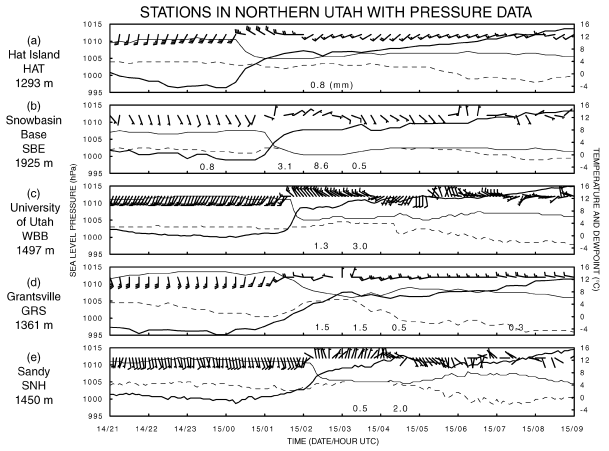


FIG. 9. Time series from (a) Hat Island (HAT, 1293 m), (b) Snowbasin Ski Resort base (SBE, 1925 m), (c) William Browning Building, University of Utah (WBB, 1497 m), (d) Grantsville (GRS, 1361 m), and (e) Sandy (SNH, 1450 m). Sea level pressure (hPa, black solid lines), temperature (°C, gray solid lines), dewpoint temperature (°C, gray dashed lines), 1-h precipitation amount (mm, numbers along bottom), and wind (one pennant, full barb, and half-barb denote 25, 5, and 2.5 m $s^{-1}$, respectively).

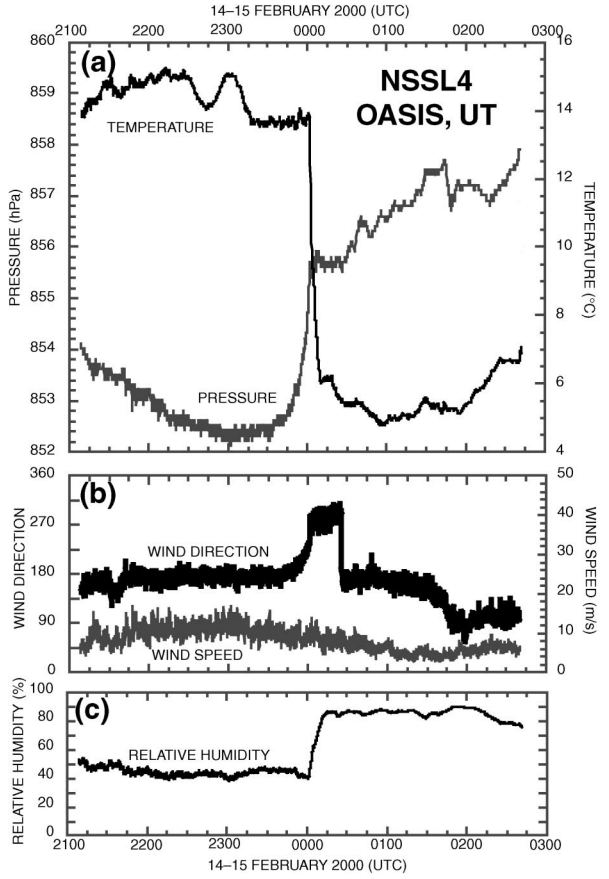


FIG. 10. Time series at NSSL4 at Oasis: (a) temperature (°C, black line) and surface pressure (hPa, gray line), (b) wind direction (°, black line) and wind speed (m $s^{-1}$, gray line), and (c) relative humidity (%, black line).

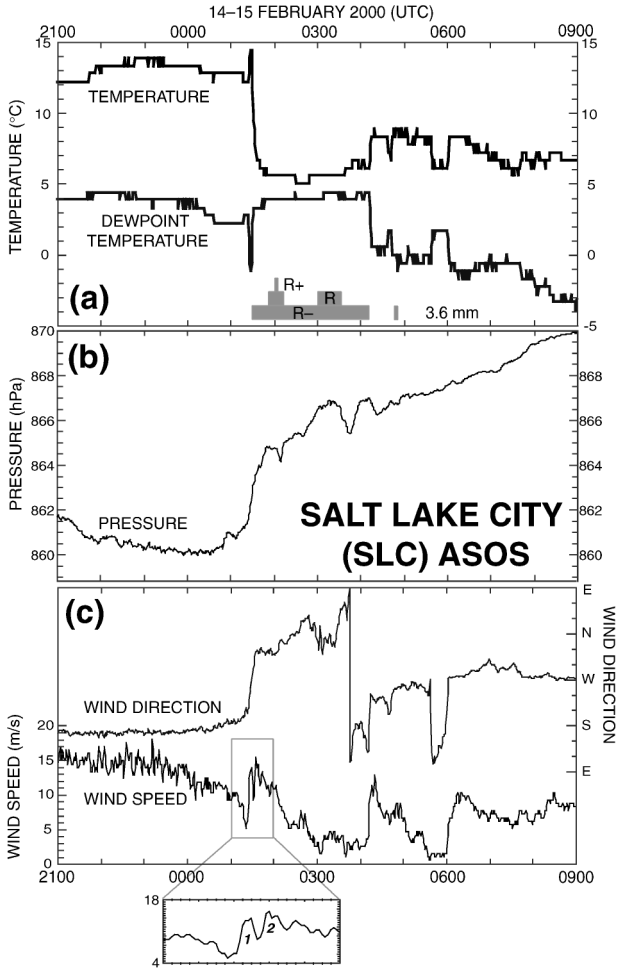


FIG. 11. Time series at Salt Lake City (SLC) Automated Surface Observing Station (ASOS) with 1-min resolution data: (a) temperature (°C, black line), dewpoint temperature (°C, gray line), observed weather (intensity of rain is proportional to height of gray boxes along bottom), and total precipitation (3.6 mm) along bottom; (b) surface pressure (hPa, black line); and (c) wind direction (gray line) and wind speed (m $s^{-1}$, black line). Inset represents expanded view of wind speed during 0100–0200 UTC. Here 1 and 2 represent maxima of wind speed discussed in section 4a.

the wind at NSSL4 was from the west, lasting only about 20 min before returning to the south-southeast again. During the 20 min of westerlies, pressure remained fairly constant, despite its rapid rise in advance of the frontal passage. The northerlies at SLC, however, lasted for over 2 h (Fig. 11c), perhaps due to either the evolution of the front or terrain channeling by the adjacent Wasatch Mountains.

Near the end of the available observations at 15/0240 from NSSL4, the temperature rose, the relative humidity decreased, and the winds became more easterly (Fig. 10). Similar behavior occurred at SLC, where the postfrontal period of low temperatures and high dewpoints was associated with 3.6 mm (0.14 in.) of rain (Fig. 11). The reason for this behavior is discussed further later in this paper.

Finally, a prefrontal temperature undulation occurred between 14/2230 and 14/2315 with a half-period (time from minimum to maximum in temperature) of nearly 15 min at NSSL4 (Fig. 10a). A similar feature appeared to be indicated in the data from MesoWest stations reporting every 5 min (e.g., IPX5, IPX6, and IPX9; not shown), but not in the SLC ASOS data (Fig. 11). [An alternative explanation for the 2.2°C temperature spike before frontal passage in Fig. 11 is provided in section 4b.] A very small relative maximum in wind speed and relative minima in pressure and relative humidity occurred at the temperature maximum of the undulation, although little change in wind speed or direction was observed with the undulation (Fig. 10). The 14/2347 sounding from NSSL4 (Fig. 16a) indicated a weak and very shallow surface-based inversion. This surface-based inversion was 50 m thick over which the temperature increased 0.7°C. That the magnitude of the surface temperature undulation in Fig. 10a (1.0°C) was nearly consistent with the potential temperature change across the inversion (1.1°C) suggests that this inversion served as the stable layer upon which this apparent solitary gravity or buoyancy wave traveled. That the inversion was not present in the earlier 14/2106 NSSL4 sounding (Fig. 16a) indicates that the surface cooling might have been due to shading of incoming solar radiation by forward-sloping cloud in advance of the convective line. This hypothesis is supported by visible satellite imagery showing clouds arriving over NSSL4 between 14/2230 and 14/2300 (not shown) and pyranometer data from Aragonite (ARAU1) showing a reduction of about 50–80 W $m^{-2}$ compared to the maximum possible solar radiation (M. Splitt 2003, personal communication). The surface inversion may also have been a result of normal nocturnal cooling, as some, but not all, 0000 UTC soundings from National Weather Service stations taken on very dry days during IPEX show such structure. Brundidge (1965; Figs. 3, 5, and 7) observed some nonnocturnal, 50–100-m-thick, surface-based, stable layers ahead of surface frontal passages in Texas, but his observations did not address the origin of such stable layers, however.

An alternative hypothesis is that this feature might be an internal bore (e.g., Simpson 1997, 21–27). Bores, however, are associated with an increase in temperature after their passage. Since the surface temperature decreased 2.3°C after the undulation (Fig. 10a), rather than increased, this undulation is unlikely to be an internal bore. Another hypothesis is that the stable layer originated over the cooler Great Salt Lake. Unfortunately, the density of high-resolution surface or upper-air measurements is inadequate to test this hypothesis.

### *c. Vertical structure of the front*

Because of the pronounced orography in northern Utah, nearby stations at different elevations can be used to examine the vertical structure of the front. For ex-

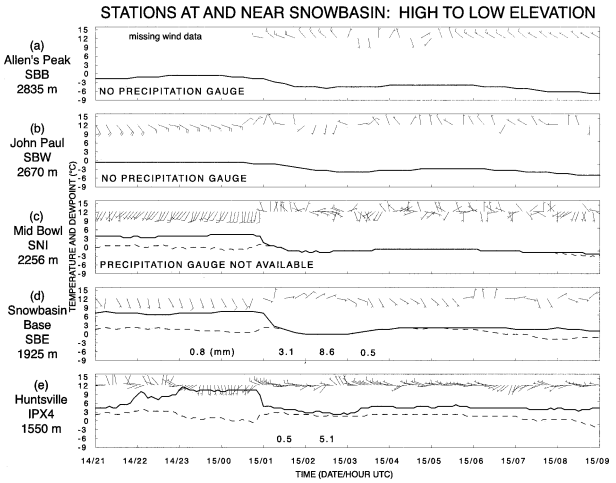


FIG. 12. Time series from five stations at and near Snowbasin Ski Resort: (a) Allen's Peak (SBB, 2835 m), (b) John Paul (SBW, 2670 m), (c) Mid Bowl (SNI, 2256 m), (d) Snowbasin Ski Resort base (SBE, 1925 m), and (e) Huntsville (IPX4, 1550 m). Temperature (°C, solid lines), dewpoint temperature (°C, dashed lines), 1-h precipitation amount (mm, numbers along bottom, unless otherwise noted), and wind (one pennant, full barb, and half-barb denote 25, 5, and 2.5 m $s^{-1}$, respectively). Reliable wind speeds are missing at SBB before 15/0100.

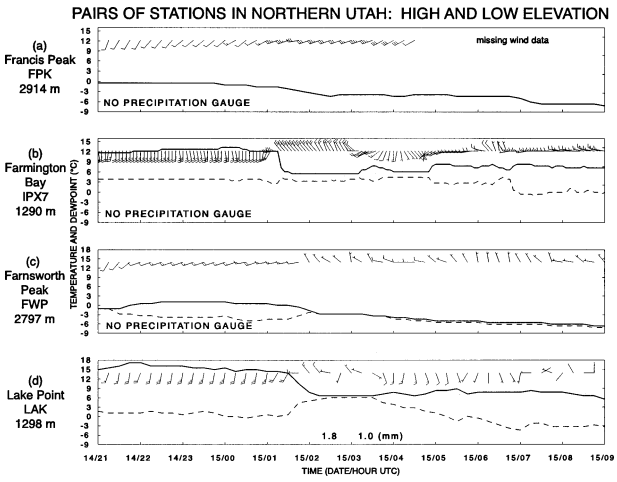


FIG. 13. Time series from (a) Francis Peak (FPK, 2914 m), (b) Farmington Bay (IPX7, 1290 m), (c) Farnsworth Peak (FWP, 2797 m), and (d) Lake Point (LAK, 1298 m). Temperature (°C, solid lines), dewpoint temperature (°C, dashed lines), 1-h precipitation amount (mm, numbers along bottom, unless otherwise noted), and wind (one pennant, full barb, and half-barb denote 25, 5, and 2.5 m $s^{-1}$, respectively). Reliable wind speeds are missing at FPK after 15/0445.

ample, one cluster of stations ranged from Huntsville (IPX4, 1550 m) to four stations at Snowbasin Ski Resort: base (SBE, 1925 m), Mid Bowl (SNI, 2256 m), John Paul (SBW, 2670 m), and Allen's Peak (SBB, 2835 m) (Fig. 12). Although these stations are not in a line up the mountain, the four Snowbasin sites are all within 5 km of each other, with IPX4 less than 15 km away (Fig. 1b). Time series from these stations show that the drop from maximum to minimum temperature associated with the front decreased with height from 9.5°C at IPX4 to 4.4°C at SBB (Fig. 12). At the lowest two stations (IPX4 and SBE), the temperature recovered more than 2°C within 2 h after the time of minimum temperature, whereas temperature recovered only 1.1°C at the higher-elevation stations.

Similarly, other pairs of stations throughout northern Utah show a large temperature recovery at low-elevation stations and a continuous decrease of temperature at high-elevation stations (Fig. 13). For example, Francis Peak (FPK, 2914 m) and Farnsworth Peak (FWP, 2797 m) both had gentle temperature decreases (4°–6°C in 5 h) with no postfrontal temperature rises, whereas adjacent low-elevation stations Farmington Bay (IPX7, 1290 m) and Lake Point (LAK, 1298 m) had abrupt temperature decreases (5.8° and 8.9°C in 1.5 h, respectively) with modest postfront temperature rises (2.8° and 2.6°C in 2 h, respectively).

This point is further illustrated by plotting the nonzero temperature drops and rises for selected stations as a function of elevation (Fig. 14). Stations below about 2200 m experienced large temperature drops (6°–10°C) with the largest values (>8°C) at the lowest elevations. Above 2200 m, the temperature drops were generally modest (4°–6°C). Similarly, the temperature rises were 1°–4°C for stations below 2200 m, but were 1°C or less for stations above 2200 m.

A final observation about the temperature change with height is that the temperature drop started earlier and lasted longer at the higher elevation stations (Figs. 12

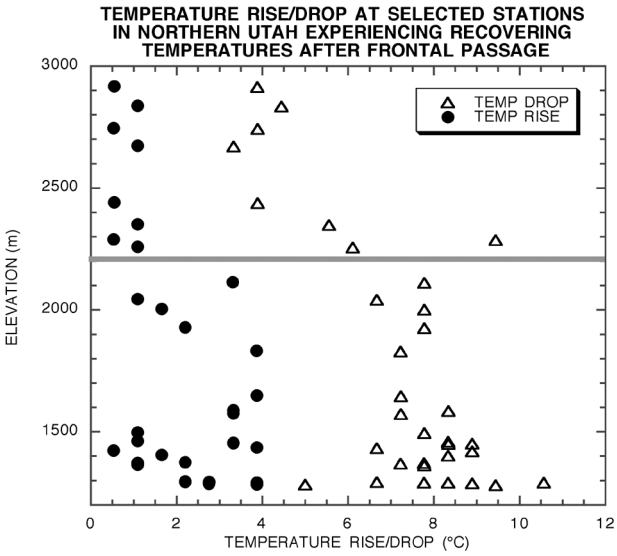


FIG. 14. Temperature drop (°C, open triangles) and temperature rise (°C, solid circles) vs elevation (m) for selected stations in northern Utah that experience recovering temperatures after frontal passage. Changes in temperature were calculated from relative maximum and minimum temperatures at each station between 14/2100 and 15/0900. Line at 2200 m represents change in the temperature drops/rises with height discussed in text.

and 13). For example, the surface temperature started falling at SBB (2835 m) after 15/0000, SBW (2670 m) after 15/0030, SNI (2256 m) after 15/0045, and SBB (1925 m) after 15/0100 (Fig. 12). Thus, roughly an hour passed between the start of the temperature drop at higher- and lower-elevation stations. Not only did the temperature fall occur earlier aloft, but the majority of the temperature decrease occurred over a longer time aloft (about 2 h) compared to that at lower-elevation stations (about 30 min) (Fig. 12). Other high-elevation stations (FPK and FWP) and nearby low-elevation stations (IPX7 and LAK) show similar behavior (Fig. 13). These observations suggest that the cold air aloft arrived before that at the surface and continued even after surface temperatures at the lower-elevation stations had become steady.

### *d. High temporal resolution soundings*

An overview of the frontal passage is shown by a time–height section constructed from special 3-hourly soundings released by the National Weather Service Forecast Office in SLC during IPEX IOP 4 (Fig. 15). This section shows the development of the prefrontal environment, including the warming and deepening well-mixed boundary layer from 14/1200 to 15/0000 and the arrival of less stable, drier air aloft (700–350 hPa) after 14/1800. (This dry air has important consequences to the frontal structure, as described later in the paper.) Surface frontal passage at SLC occurred at 15/0130 (Fig. 11), followed by the arrival of shallow cold air below 700 hPa, and near-surface warming after 15/0300, associated with the advection of drier lower-tropospheric air (Fig. 15). Aloft, the tropopause lowered from above 200 hPa at 14/1200 to about 300 hPa at 15/1200, with an upper-level frontal zone passing overhead about 15/0000 (Fig. 15). Thus, the baroclinicity associated with the lower-tropospheric front can be viewed as two components. A midtropospheric baroclinic zone ($\theta$ = 300–308 K) between 800 and 400 hPa at 15/0000–15/0600 represents the passage of the shortwave trough aloft, whereas the cold pool near the surface after 15/0130 ($\theta$ = 292–298 K) represents the diabatically cooled, moist downdraft air (Fig. 15).

A more detailed picture of the frontal passage can be obtained by analyzing soundings released from the two NSSL mobile laboratories: NSSL4 at Oasis and NSSL5 at Ogden-Hinckley Airport (OGD, see Fig. 1a for their locations). The first pair of soundings, released ahead of the surface frontal passage at 14/2106 by NSSL4 and 14/2142 by NSSL5, show midtropospheric dry air and well-mixed boundary layers (Figs. 16a,b). Winds at NSSL4 were nearly unidirectional from the west-southwest above 700 hPa. In contrast, winds at NSSL5 exhibited a bit more veering and lighter speeds below about 600 hPa, perhaps due to the nearby Wasatch Mountains decelerating the wind and turning it to a more mountain-parallel component below crest level (~700 hPa), also observed during an earlier IPEX event (Cox 2002).

Fifteen minutes before the surface frontal passage at NSSL4 (14/2347), the well-mixed boundary layer had warmed and dried below 714 hPa and deepened to 680 hPa (Fig. 16a), with a moist layer above. A similar moist layer occurred above 475 hPa at NSSL5 at 14/2328 (Fig. 16b). These moist layers are indicative of prefrontal clouds arriving aloft, as discussed earlier from the satellite imagery (not shown) and as to be shown from radar data in section 4. Cooling of 1°–3°C occurred at NSSL4 from 714 hPa to nearly 300 hPa (Fig. 16a), thus decreasing stability, consistent with the LKN and SLC soundings (Fig. 4). CAPE at NSSL4 at 14/2347 was 120 J kg$^{-1}$ with 22 J kg$^{-1}$ of convective inhibition. Less cooling and destabilization occurred at NSSL5 at 14/2328, however, with CAPE of 85 J kg$^{-1}$ and CIN of 69 J kg$^{-1}$ (Fig. 16b). Although CAPE was small, the strong vertical wind shear at NSSL5 at 14/2328 (0–3-km AGL shear of 35 m s$^{-1}$ and 0–5-km AGL shear of 39 m s$^{-1}$) indicated an enhanced potential for organized severe weather, consistent with the strong wind gusts observed throughout northern Utah (Fig. 2).

A third pair of soundings was released from NSSL4 and NSSL5 after frontal passage (Figs. 16c,d). Although the soundings were relatively unchanged above 650 hPa at NSSL4 and above 500 hPa at NSSL5, cloud base had lowered to about 700 hPa or −2°C. Significantly, cooling of up to 8°C and moistening of up to 1.5 g kg$^{-1}$ occurred in the lowest levels, suggesting sublimating/evaporating precipitation falling from cloud base, but beginning as snow. Unfortunately, direct observations of precipitation starting aloft and descending with time to support this hypothesis are not available due to nonexistent or nonoperating precipitation sensors at high-elevation stations and the 1-h or greater sampling rate of these sensors.

The last soundings from the mobile laboratories were released around 15/0230 (Figs. 16c,d). The sounding from NSSL4 showed cooling of 2°–5°C between 700 and 500 hPa, warming of 1°–3°C below 750 hPa, and strong drying below 550 hPa, producing a sounding with two dry layers separated by a moist layer (Fig. 16c). Such a ''double-onion'' structure has also been noted by Zipser (1969, 1977), Stumpf et al. (1991), and Knievel (2001). In this case, the lower onion (dry region below 600 hPa in Fig. 16c) represents rear-to-front dry inflow air originating outside of the frontal circulation since its $\theta_e$ (304–308 K) is lower than any prefrontal air that could have been involved in the convection ($\theta_e \geq$ 310 K; cf. Figs. 16a,c). If the arrival of this drier air at low levels is related to the drying observed at surface stations (e.g., Figs. 7a–c), then, at some stations, the dry air appears to arrive in spurts (e.g., Fig. 13b). The reason for the upper onion (dry region above 500 hPa in Fig. 16c) is unclear. By comparison, the sounding from NSSL5 remained nearly saturated throughout its

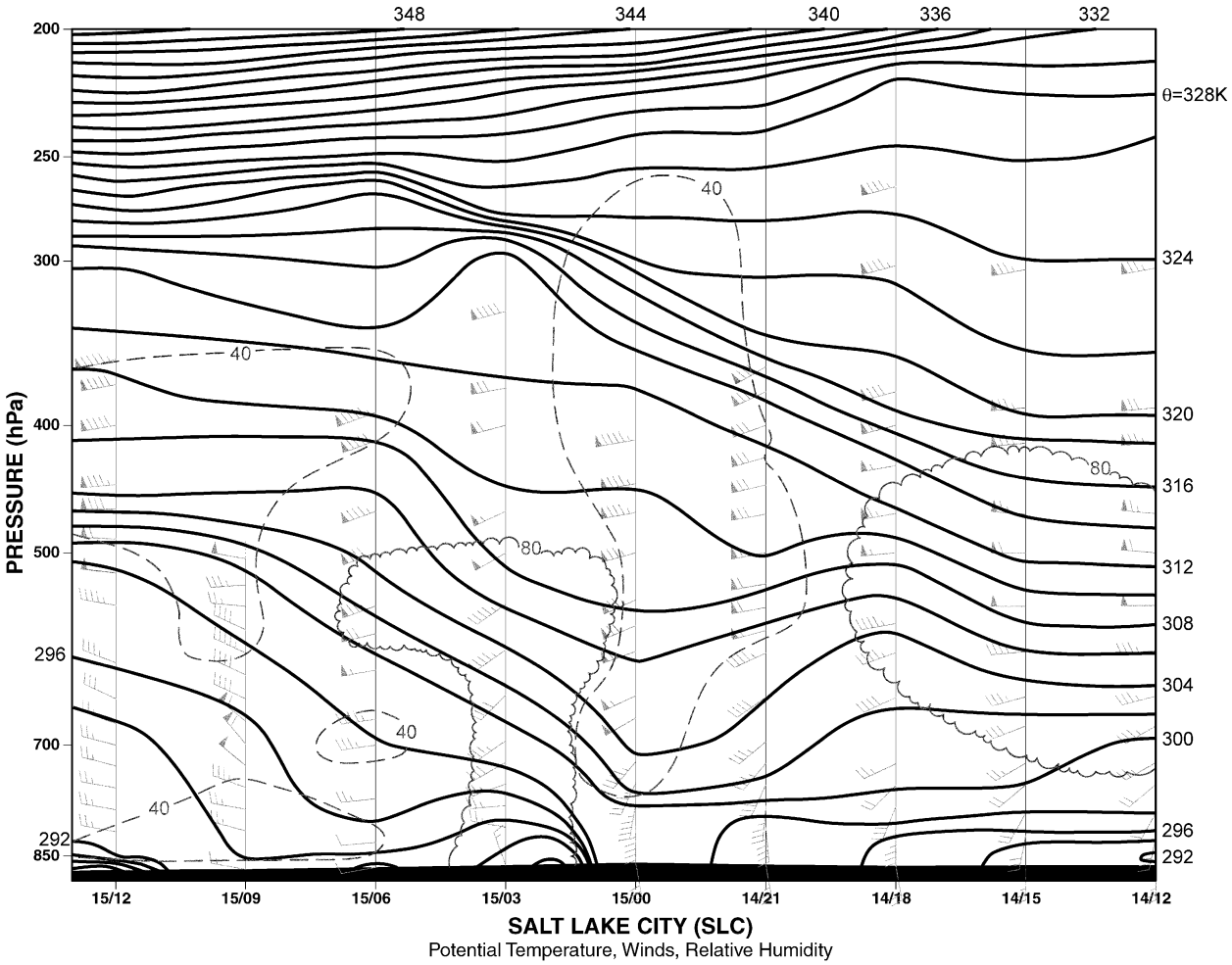


FIG. 15. Time–height section of 3-h soundings at Salt Lake City (SLC) from 14/1200 to 15/1200. Potential temperature (solid lines every 2 K), relative humidity less than 40% (gray dashed lines), relative humidity greater than 80% (gray scalloped lines), and wind (one pennant, full barb, and half-barb denote 25, 5, and 2.5 m $s^{-1}$, respectively). Times of soundings are related to their synoptic times, rather than the balloon release times as has been convention throughout the rest of the paper.

depth, albeit with 1°–2°C cooling below about 600 hPa (Fig. 16d).

In addition to soundings from the mobile laboratories, a 924-MHz wind profiler (DPG), maintained by the U.S. Army Dugway Proving Grounds south and west of the Great Salt Lake, also captured the frontal passage (Fig. 17). Whereas the wind shift from southwest to northwest occurred at nearby surface station Target S (DPG04) between 15/0230 and 15/0245 (not shown), the DPG winds at 1436–2206 m MSL had already shifted from the southwest to the west by 15/0205 (Fig. 17). Surface observations as a function of elevation discussed earlier in this paper (Figs. 12 and 13) did not possess a wind shift aloft before that at the surface, and the soundings from the mobile laboratories (Fig. 16) were too infrequent to address this question. We speculate that the arrival of the westerlies aloft before those at the surface is likely a result of surface friction retarding the front in the lowest 50–100 m, as shown by previous observational (e.g., Berson 1958; Brundidge 1965; Shapiro 1984) and modeling (e.g., Tory and Reeder 1996) studies.

The importance of the precipitation to the kinematics and dynamics of this front have already been hinted at in regard to the subcloud cooling and moistening due to sublimation. Therefore, to understand the cloud and precipitation structure in more detail, we next examine high-resolution radar data.

## 4. DOW radar analysis

Although the NOAA P-3 research aircraft was deployed during IPEX, problems with its tail radar did not permit it to fly during IOP 4. One of the University of Oklahoma Doppler on Wheels mobile radars (Wurman et al. 1997), DOW3, was unavailable due to a nonfunctioning antenna motor. Nevertheless, DOW2, the other DOW deployed during IPEX, was operating dur-

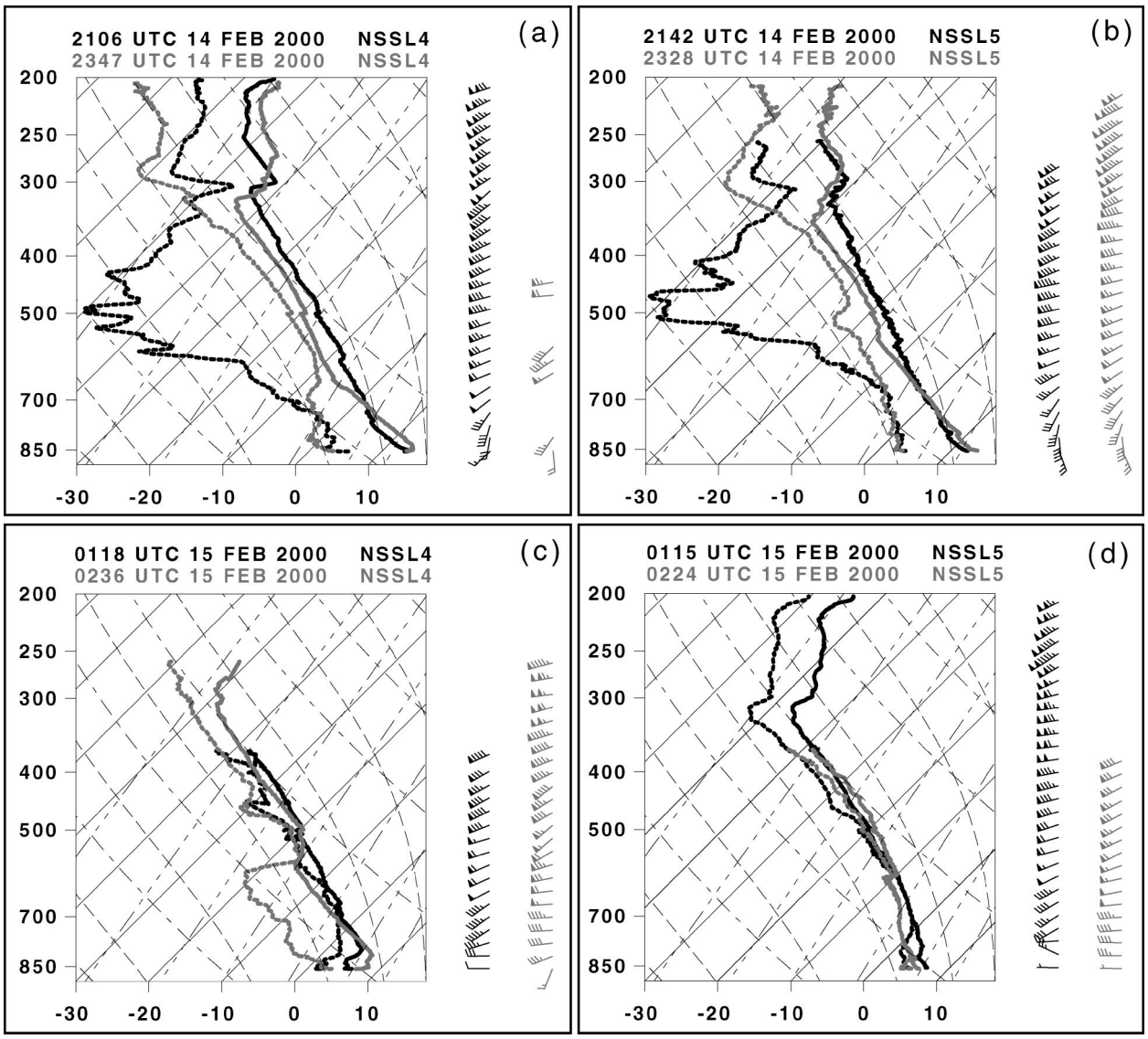


FIG. 16. Skew *T*–log*p* plot of observed soundings released from (a), (c) NSSL4 and (b), (d) NSSL5. (a) 2106 UTC 14 Feb (black) and 2347 UTC 14 Feb (gray) at NSSL4, (b) 2142 UTC 14 Feb (black) and 2328 UTC 14 Feb (gray) at NSSL5, (c) 0118 UTC 15 Feb (black) and 0236 UTC 15 Feb (gray) at NSSL4, and (d) 0115 UTC 15 Feb (black) and 0224 UTC 15 Feb (gray) at NSSL5. Temperature (°C, solid lines), dewpoint temperature (°C, dashed lines), and winds (one pennant, full barb, and half-barb denote 25, 5, 2.5 m $s^{-1}$, respectively). The data is 1-s sampling-interval format and is processed using a methodology similar to that of Williams et al. (1993).

ing this event and was situated on the east side of the Great Salt Lake at Syracuse, Utah (1280 m MSL, see Fig. 1 for the location of DOW2). DOW2 started scanning at 15/0045, right after frontal passage, and continued until 15/0322.

### *a. PPIs*

The earliest scan, beginning 15/0045, shows a sharp wind shift and wind maximum just a few kilometers southeast of DOW2 (the arrow labeled 1 in Fig. 18b). In the 2.5°-elevation plan position indicator (PPI), the leading edge of the several-kilometer-wide band of weakly convective precipitation trails the wind shift by about 5 km (cf. Figs. 18a,b). Coincident with the precipitation is a secondary radial wind speed maximum, west of DOW2 (the arrow labeled 2 in Fig. 18b). This double maximum in radial wind speed is more easily seen at 15/0050 after both maxima have nearly doubled in magnitude and passed DOW2 (Fig. 18d). This structure persisted for roughly another 5 min, and then was no longer resolved in the DOW2 PPIs. This double-wind structure was also observed with the 1-min ASOS data from SLC (Fig. 11c). Whereas the first wind speed maximum was associated with the leading edge of northwesterly wind, the second maximum was associated with the onset of

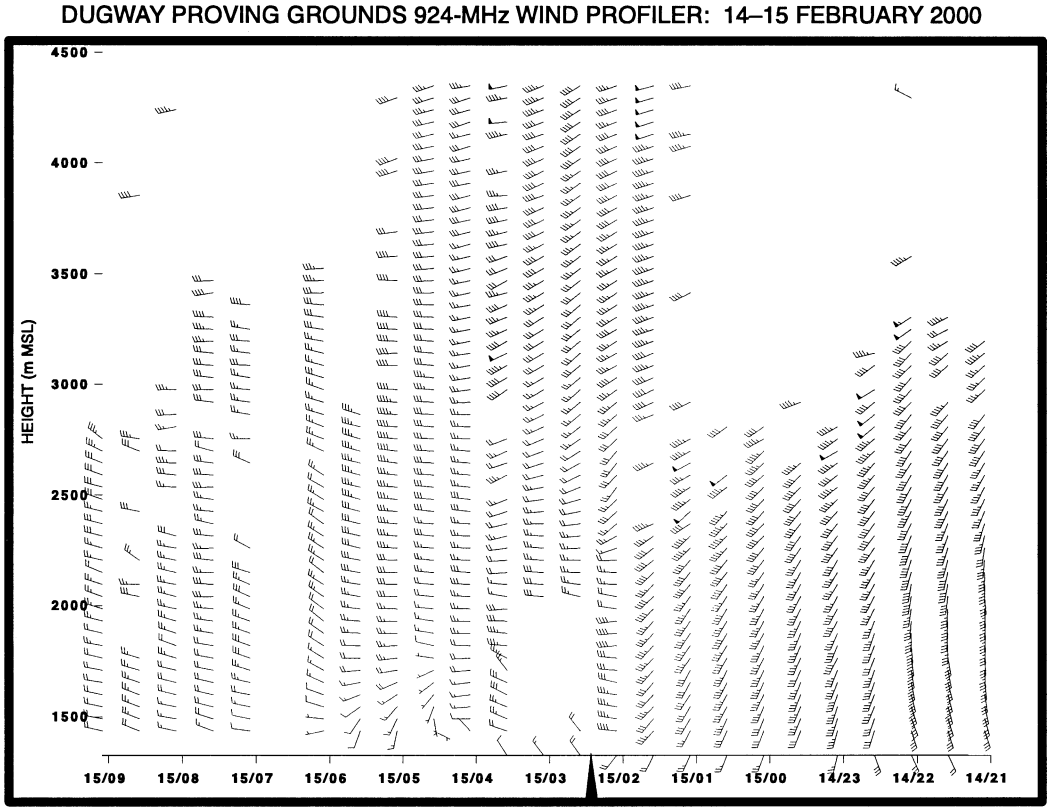


FIG. 17. Time–height section of winds (one pennant, full barb, and half-barb denote 25, 5, 2.5 m $s^{-1}$, respectively) with height (m MSL) from the U.S. Army Dugway Proving Grounds 924-MHz wind profiler (DPG) from 2105 UTC 14 Feb to 0905 UTC 15 Feb. Triangle represents time of surface frontal passage.

precipitation at the surface. Thus, the PPIs—and the double maximum in radial wind speed, in particular—further suggest the importance of diabatic processes to the microscale structure of the cold front.

After moving past DOW2, the convective line stalled and its associated precipitation became less organized (Figs. 18e,g). The post-convective-line showers, earlier moving from the northwest, began moving from the southwest and eventually west (not shown), parallel to the line and the flow aloft (e.g., the 14/2313 SLC sounding in Fig. 4b and Fig. 18f). By 15/0235, the lower-tropospheric flow north of the front became more westerly (Fig. 18h), or roughly perpendicular to the crest of the Wasatch, resulting in the development of 30 m $s^{-1}$ westerly gap flow through Weber Canyon (Fig. 18h). The stronger wind speed west of DOW2 than east of DOW2 (Fig. 18h) implied blocking and deceleration of about 5 m $s^{-1}$ as the westerlies approached the mountains, consistent with the NSSL4 and NSSL5 soundings discussed earlier (Figs. 16a,b) and research performed on an earlier event during IPEX (Cox 2002). At a height of 2–3.5 km MSL (equivalent to a range of 10–30 km in Fig. 18h), however, confluence was occurring with westerlies north of DOW2 and southwesterlies south of DOW2 in this layer (Fig. 18h), consistent with the westerly winds at NSSL4 and NSSL5 around 15/0230 (Figs. 16c,d) and southwesterlies at DPG at 15/0230 (Fig. 17) and SLC at 15/0300 (Fig. 15). The significance of this postfrontal confluence is the subject of future research.

### *b. RHIs*

The vertical structure of the frontal system can be examined in range–height indicators (RHIs) from DOW2. An RHI from 15/0104 (Fig. 19a) shows the forward-sloping cloud previously identified from the soundings (Fig. 16), with lobes of higher radar reflectivity underneath, about 1–2 km in diameter. These lobes of radar reflectivity agree with observations of virga and mammatus ahead of the front by an off-duty IPEX forecaster who was in the Wasatch Mountains at this time (J. LaDue 2000, personal communication). The 14/2347 prefrontal sounding from NSSL4 showed a superadiabatic layer (lapse rate of 12.6°C $km^{-1}$ over a depth of 246 m between 681 and 660 hPa at temperatures of −2.0 to −5.1°C, respectively) before the sonde penetrated the cloud (Fig. 16a). Below the superadiabatic layer, a layer from 681 to 698 hPa with near constant mixing ratio, potential temperature, and equivalent potential temperature resembling the early stages of an

''onion sounding'' suggests a sublimation-initiated downdraft was occurring (e.g., Stensrud et al. 1991, p. 2132; Parker and Johnson 2003c, manuscript submitted to *J. Atmos. Sci.*, hereafter PJc). Further evidence for this downdraft comes from the time series of temperature at the SLC ASOS showing a 2.2°C temperature rise and 3.9°C dewpoint drop in 4 minutes immediately before surface frontal passage (Fig. 11a), suggesting that, at this time, adiabatic warming due to descent was dominating diabatic cooling due to sublimation/evaporation, as discussed by Gilmore and Wicker (1998). The presence of the mammatus and the subcloud thermodynamic structure is evidence for subcloud diabatic cooling from the sublimation of snow.

At 15/0109, the forward-sloping cloud layer and subcloud sublimation were apparent, as was the developing melting layer (the ''bright band'' about 1 km AGL or 2.3 km MSL) to the rear of the system (Fig. 19b). Observations of the rain–snow transition at about 2.1 km MSL from surface station reports of precipitation type (not shown) and the height of the 0°C isotherm in the soundings (Figs. 16c,d) support this interpretation. The transition to postfrontal stratiform cloud [defined by Houze (1997, Fig. 1) as the presence of bright banding and weak horizontal gradients in radar reflectivity factor] occurred within only 6 km (Fig. 19b), consistent with idealized model simulations of precipitating cold fronts (e.g., Barth and Parsons 1996) and indicating the small spatial scale of the precipitation structure of the cold front. By 15/0146, the showery precipitation (e.g., Fig. 18e) was classified as stratiform due to the layered radar reflectivity pattern, bright banding, and fall streaks (Fig. 19d).

In the accompanying velocity field at 15/0109 (Fig. 19c), the leading edge of the northwesterlies and the shallowness of the flow (500–1000 m AGL) were apparent. The low-level flow behind the wind shift line was about 21 m $s^{-1}$ (Fig. 19c), which was much greater than the 12 m $s^{-1}$ speed of the wind shift line (computed from radar PPIs over the 10 minutes starting at 15/0045). This characteristic head to the velocity pattern and 9 m $s^{-1}$ rear-to-front flow at low levels imply that the front possessed characteristics of a gravity current (e.g., Smith and Reeder 1988). As will be shown shortly, other evidence supports the similarity of this case to a gravity current, also.

### *c. Cross sections from CAPPIs*

To examine further the structure of the front as it passed DOW2, constant-altitude plan position indicators (CAPPIs) were created from the radar reflectivity factor and radial velocity from DOW2. These raw radar data were interpolated to a uniformly spaced Cartesian grid of horizontal and vertical gridpoint mesh lengths equal to 0.5 and 0.25 km, respectively. The interpolation procedure involved a single-pass Barnes (1964) objective analysis scheme with a dimensional smoothing parameter of 0.24 $km^2$, as per Trapp and Doswell (2000). Vertical cross sections were then formed from these gridded data (Fig. 20), as proxies to actual RHIs not collected during this period.

Northwest–southeast cross sections perpendicular to the cold front show that the strong gradient in wind speed associated with the surface wind shift was initially vertical through at least 2.3 km MSL (1 km AGL) at 15/0045 (Fig. 20a). The horizontal convergence normal to the front was about $8 \times 10^{-3}$ $s^{-1}$ at this time, giving a rough estimate of vertical velocity at 1 km AGL from the continuity equation of 8 m $s^{-1}$. Relatively shallow, convective vertical velocities of this magnitude have also been shown in fronts analyzed by Browning and Harrold (1970), Carbone (1982), and Shapiro (1984), for example.

Within the next 3 minutes, the magnitude of the maximum wind speed doubled behind the wind speed gradient (cf. Figs. 20a,c). Two maxima of wind speed near the surface became apparent, consistent with the two maxima discussed earlier (e.g., Figs. 11c and 18b,d). An increase in radar reflectivity factor associated with the second wind maximum (cf. Figs. 20b,d) supports the hypothesis that its origin was associated with a precipitation-laden downdraft. Over time (Figs. 20e,g,i), the two maxima in wind speed separated from each other as the front evolved into a structure reminiscent of a gravity current. The black line in Figs. 20c,e,g,i represents the line of zero front-relative flow, calculated by subtracting 12 m $s^{-1}$ from the radial winds observed by DOW2. This position of this line indicates a substantial depth was rear-to-front flow, a principal requirement for gravity-current flow. Carbone (1982) and many others have shown similar structures in their observational studies of precipitating and nonprecipitating cold fronts. [See Smith and Reeder (1988) for a more detailed review of cold fronts as gravity currents.]

Thus, the initially vertical, radial-velocity gradient (Fig. 20a) evolved into a feature reminiscent of a gravity current, with the rear-to-front, front-relative flow from the radar thinning to only 0.5–0.7 km AGL by 15/0055 and 15/0100 (Figs. 20g,i). Why the evolution occurred at this particular time is unknown. Likely, the evolution was due to a localized downdraft, fortuitously observed by DOW2. For example, Oliver and Holzworth (1953) showed how subcloud evaporation could produce a shallowing leading edge to a precipitating front. The shallowing front in this study also recalls IPEX IOP 7 on 24 February 2000 when an initially deep (about 4 km AGL) precipitating front over eastern Nevada thinned out to only 500 m AGL deep when it arrived at the Wasatch Mountains (Schultz et al. 2002, 203–205). The rapid evolution and shallowness of the frontal features as shown by these two IPEX IOPs indicate the difficulties researchers and forecasters confront with understanding and predicting frontal passages in the Intermountain West.

The cross sections also illustrate the forward-sloping

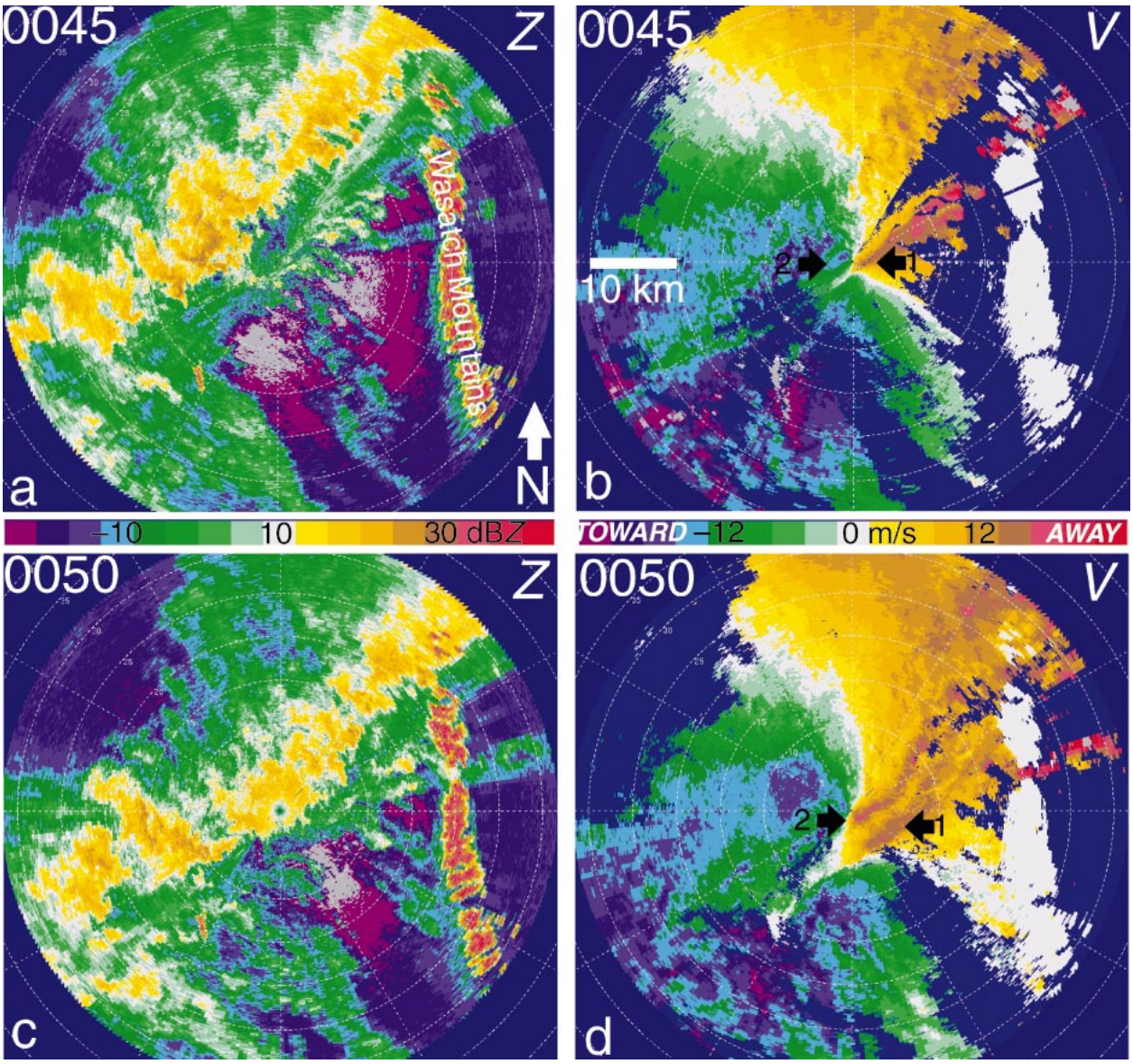


FIG. 18. PPIs at 2.5° elevation angle from DOW2: (a), (c), (e), and (g) radar reflectivity factor (dBZ) and (b), (d), (f), and (h) radial velocity (m $s^{-1}$). (a), (b) 0045 UTC 15 Feb; (c), (d) 0050 UTC 15 Feb; (e), (f) 0120 UTC 15 Feb; and (g), (h) 0235 UTC 15 Feb. (b), (d) Black arrows numbered 1 and 2 represent locations of two wind maxima discussed in text. (h) Black arrows represent the direction of the flow, showing confluence aloft. Range rings are every 5 km, starting at 10 km from DOW2.

precipitation structure (Figs. 20f,h,j). Such a structure is in contrast to the rearward-sloping precipitation structures associated with cold fronts discussed previously in the literature (e.g., Browning and Harrold 1970; Carbone 1982; Hobbs and Persson 1982). The existence of the forward slope owes to the environment of the front being characterized by small CAPE, but large wind shear. Indeed, in an environment somewhat analogously characterized by 0–5-km AGL shear of 35 m $s^{-1}$, but CAPE of 2200 J $kg^{-1}$, numerically simulated *nonfrontal* squall lines tend to be highly tilted downshear and composed of a relatively narrow band of weak cells (e.g., Weisman et al. 1988). In the present case, we believe the larger-scale lifting from the shortwave trough aloft helps maintain the integrity of the system in the presence of strong shear, as can be inferred from the idealized convective-storm simulations by Crook and Moncrieff (1988) and the squall-line case discussed by Locatelli et al. (1998).

The results of this section and the previous one (i.e., sections 3 and 4) indicate the importance of subcloud sublimation, melting, and evaporation of precipitation to the structure and evolution of the front. The next section examines how these processes affect the observed precipitation distribution.

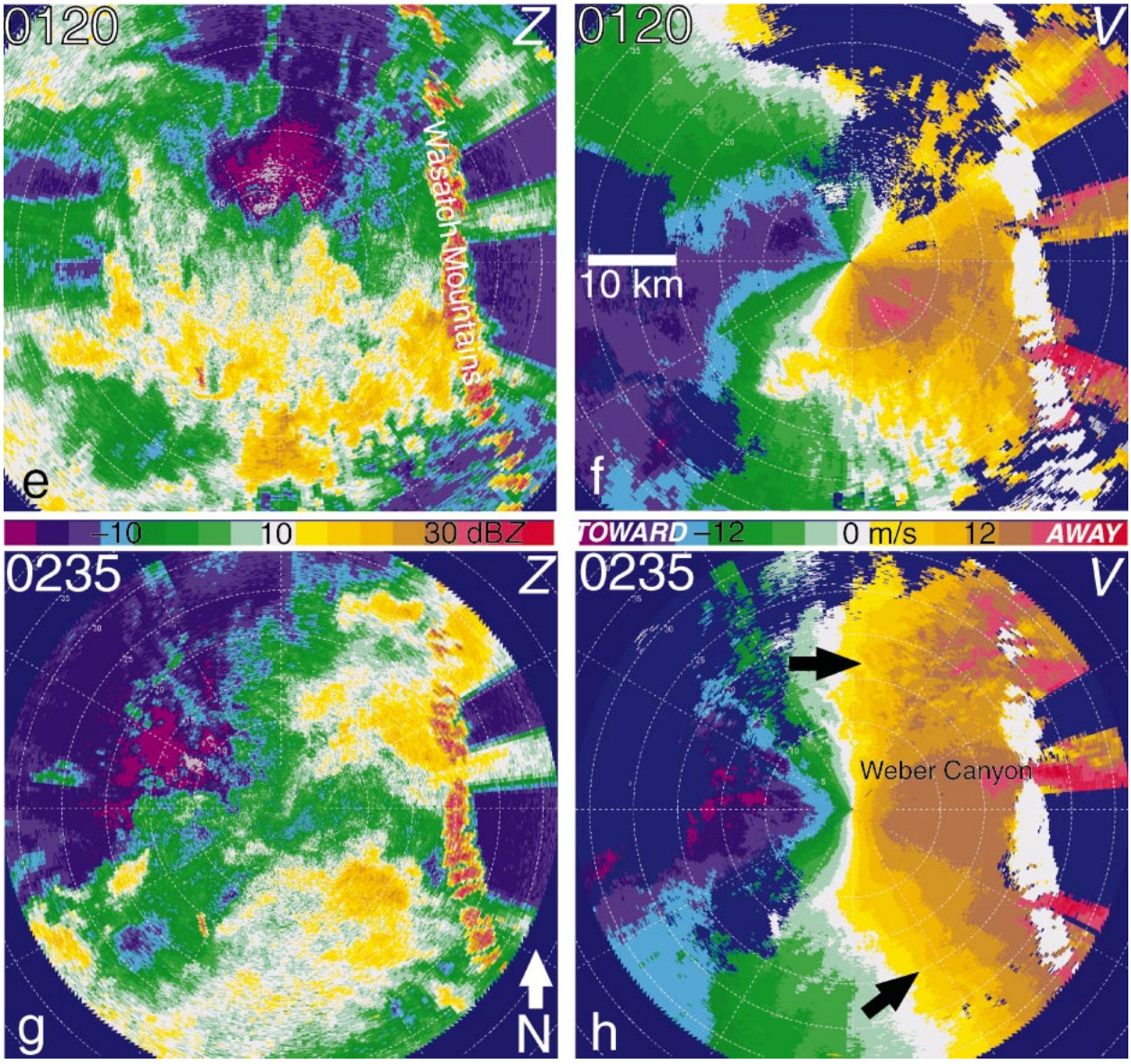


FIG. 18. (*Continued*)

## 5. Precipitation distribution

A quality-controlled precipitation dataset (Cheng 2001) is employed to understand the spatial distribution of the precipitation associated with this front. The storm-total precipitation (Fig. 21) was less than 20 mm at all sites, with a factor of two or more greater precipitation amounts in the mountains than the valley locations. The bulk of the precipitation fell during the 6 h ending 15/0600, by which point the front had passed through the northern Utah domain considered in this study (Fig. 6).

A plot of 6-h precipitation amount versus station elevation shows two distinct regions (Fig. 22). In the first region, below about 1900 m MSL, precipitation amount was less than about 7 mm and tended to increase with height, although some stations like Bountiful (SNZ) deviated from this trend due to orographic enhancement. In the second region, above about 1900 m, most precipitation amounts were greater than 7 mm, as well as much more variable. Two of these stations with lower precipitation amounts, Timpanogos Cave (TPC) and Timpanogos Divide (TIMU1), tend to be in the precipitation shadow of the Traverse Mountains in westerly and northwesterly flow. Other stations, Daniels-Strawberry (DSTU1) and Dry Bread Pond (DBPU1), are on the east side of the crest of the Wasatch Mountains, also orographically unfavorable areas for precipitation in westerly flow. Another cluster of stations above 1900 m had precipitation amounts greater than about 11 mm.

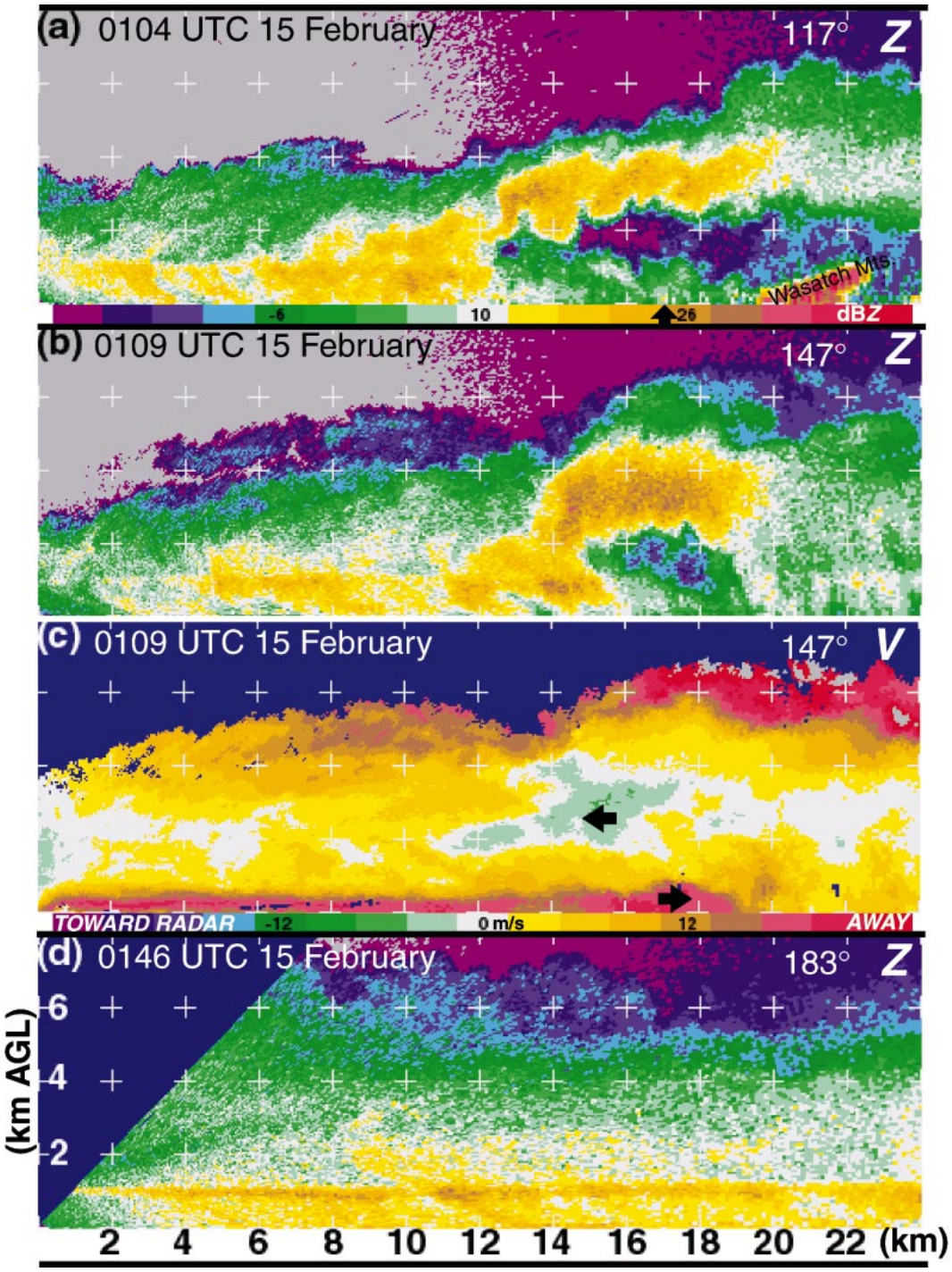


FIG. 19. RHIs from DOW2: (a) radar reflectivity factor (dBZ) at 0104 UTC 15 Feb along the 117° azimuth; arrow represents wind shift at surface in radial velocity (not shown); scale for radar reflectivity factor for (a), (b), and (d) at the bottom; (b) radar reflectivity factor (dBZ) at 0109 UTC 15 Feb along the 147° azimuth; (c) radial velocity (m $s^{-1}$) at 0109 UTC 15 Feb along the 147° azimuth; scale for radial velocity at the bottom (positive values of radial velocity represent wind moving away from DOW2 and negative values represent wind moving toward radar); wind directions noted by the black arrows; and (d) radar reflectivity factor (dBZ) at 0146 UTC 15 Feb along the 183° azimuth; numbers around edge of panel represent horizontal distance away from DOW2 (km) and vertical distance (km AGL). MSL = AGL + 1.28 km.

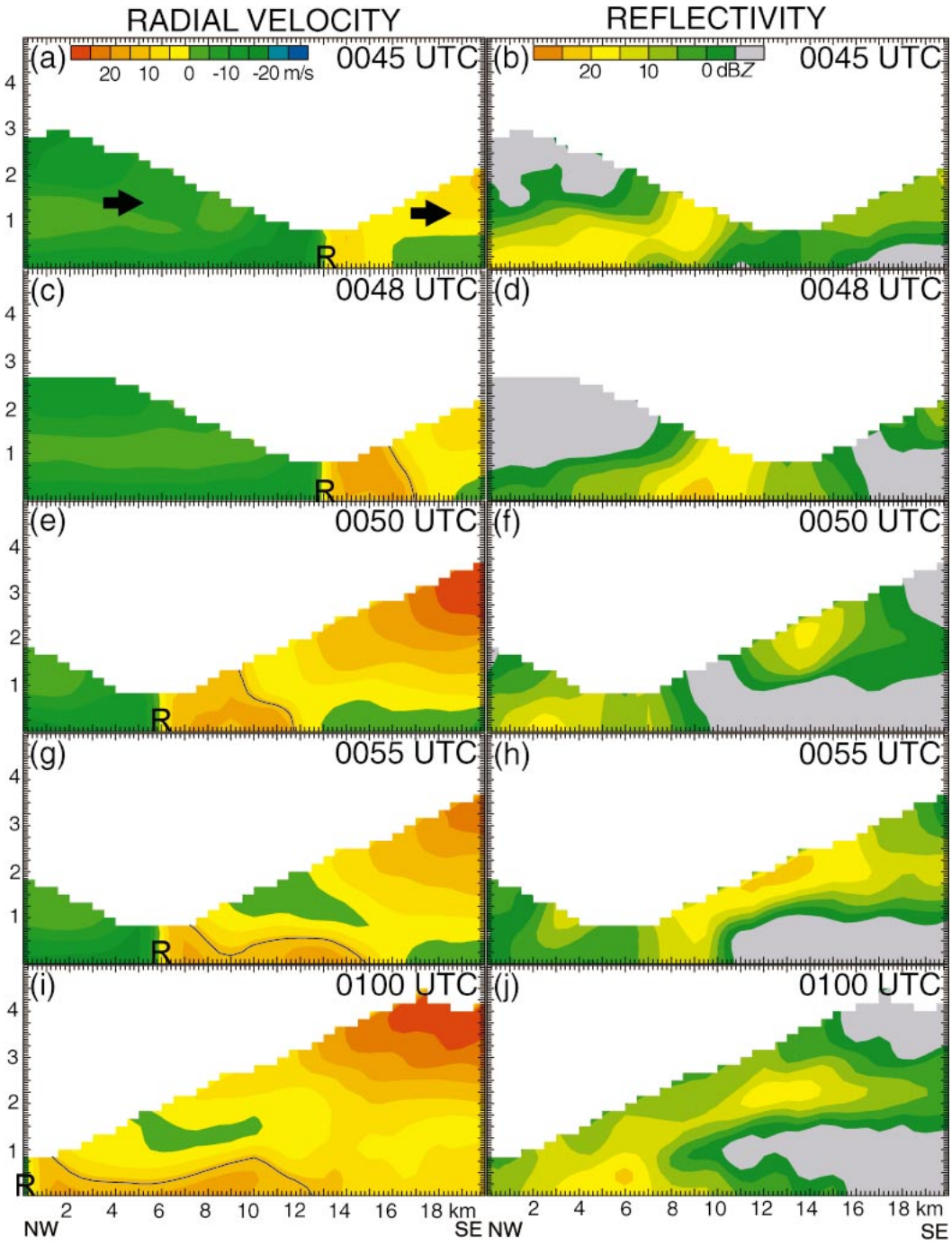


FIG. 20. Northwest–southeast (135° azimuth) vertical cross sections through CAPPIs from DOW2: (a), (c), (e), (g), and (i) radial velocity (m $s^{-1}$, shaded) and zero isopleth of front-relative velocity (black line) and (b), (d), (f), (h), and (j) radar reflectivity factor (dBZ). (a), (b) 0045 UTC 15 Feb; (c), (d) 0048 UTC 15 Feb; (e), (f) 0050 UTC 15 Feb; (g), (h) 0055 UTC 15 Feb; and (i), (j) 0100 UTC 15 Feb. Location of DOW2 identified by R in (a), (c), (e), (g), and (i). Black arrows in (a) represent the direction of the flow within the cross section. Numbers around edge of panels represent horizontal (km) and vertical scales (km AGL). Total domain size is 20 km in the horizontal and 5 km AGL in the vertical. MSL = AGL + 1.28 km.

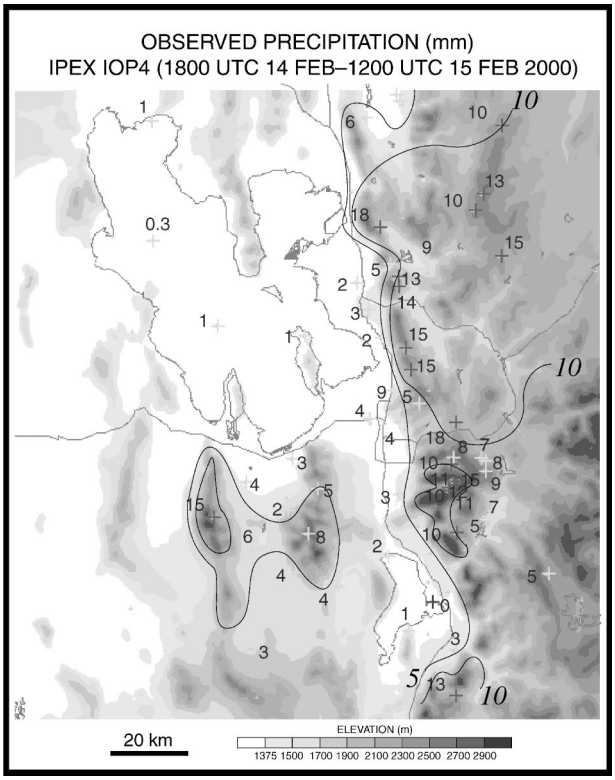


FIG. 21. Storm-total precipitation amounts (mm) for IOP 4 (1800 UTC 14 Feb–1200 UTC 15 Feb), adapted from Cheng (2001). Plus signs identify stations reporting precipitation during the period. Stations are labeled with the observed precipitation totals to the nearest whole millimeter, except for values less than 0.5 mm, which are labeled to the nearest 0.1 mm. Contours of 5 and 10 mm, where possible, are manually analyzed based upon the available data. Elevation (m) is shaded according to scale.

These stations include Brighton (BRT), Parley's Summit (PSUU1), and several stations at Snowbasin (SNI, SB1, SBE), regions that are favored for orographic enhancement in strong westerly flow because they are at, or very near, the crest of the Wasatch. In addition, Brighton and Snowbasin generally receive greater precipitation in southerly or westerly flow compared to the more climatologically favored locations Alta (e.g., CLN) and Snowbird (e.g., SBDU1, GAC; e.g., Dunn 1983; L. Dunn 2002, personal communication)—in this case about 40% more precipitation during these 6 h (Fig. 22). The remaining stations above 1900 m had precipitation amounts rather uniform with height with 7–11 mm. Thus, precipitation amounts were relatively constant with height above about 1900 m and the variability can be attributed principally to orographic influences relative to the observing site. Below 1900 m, on the other hand, the precipitation amounts were much less and increased with height. The variability of amounts at a given elevation also were small, since most stations below 1900 m were in valleys where direct orographic effects were reduced.

Nevertheless, caution should be exercised with these precipitation amounts since many of these stations (e.g., those station names ending in ''U1'') are snow telemetry (SNOTEL) stations maintained by the U.S. Department of Agriculture's Natural Resources Conservation Service (e.g., McMillan 1981). The precipitation gauges at such stations have reporting resolutions of 0.1 inch (2.54 mm) and were designed for season-total, not hourly, precipitation reporting. See Doesken and Schaefer (1987) and Gaudet and Cotton (1998, section 5) and references within for more about SNOTEL precipitation measurements.

Why does the relationship between precipitation and elevation change at about 1900 m? The sounding from NSSL5 at 15/0224 UTC shows that cloud base was roughly at this height (2137 m MSL, 792 mb, and 1.5°C), with subcloud air underneath possessing dewpoint depressions of 1°–2°C (Fig. 22). Thus, excluding stations with orographic effects, precipitation was uniform with height at the available observing stations above cloud base, whereas precipitation decreased with height below cloud base, indicating the importance of subcloud sublimation/evaporation to controlling the precipitation distribution with height.

A variety of factors appear to play a role in why the precipitation distribution was relatively simple in this case. The rapid movement of the front through northern Utah was not a complicated synoptic pattern; it also limited prolonged orographic effects, which otherwise might have complicated interpretation of the precipitation pattern. These factors imply that the effect of the subcloud sublimation/evaporation could be nearly isolated from the orographic effects. More prolonged and complicated cases, however, would be more difficult to understand. For example, Steenburgh (2003) showed that the ratio of precipitation amounts at a high-elevation station (CLN) to that at a low-elevation station (SLC) for different stages of a complex series of storms over a 4-day period in northern Utah can be quite variable, ranging from 1.25 to 14. In addition, Williams and Peck (1962) showed that this ratio for storm-total precipitation may depend on the synoptic situation.

## 6. Discussion

Throughout this paper, we have presented evidence indicating that prefrontal sublimating/evaporating precipitation was important in this case. In this section, we explore in more detail the consequences of subcloud sublimation/evaporation to the movement and the structure of this front.

### *a. Movement of the front*

The factors that control the movement of cold fronts have long been studied [e.g., Smith and Reeder (1988) and references within]. In the present case, the upper-level shortwave trough and the precipitation being formed by that synoptic-scale ascent was important to

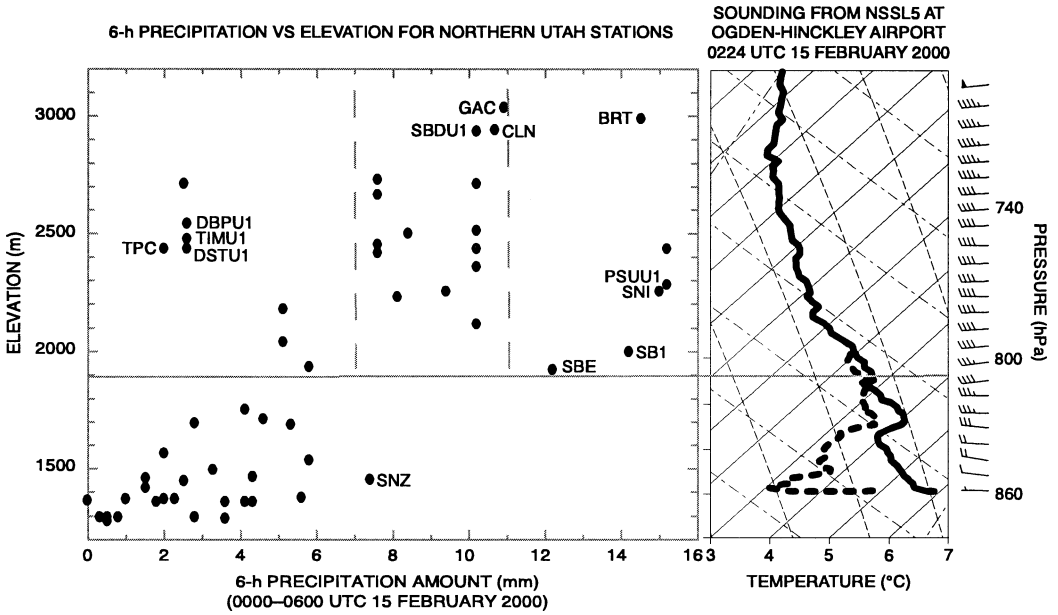


FIG. 22. (left) Precipitation amount (mm) vs elevation (m) for stations reporting precipitation during the 6 h ending 0600 UTC 15 Feb. Selected stations discussed in text are labeled. Dataset derived from the work of Cheng (2001). Gray solid and dashed lines represent boundaries between regions discussed in text. Right: skew *T*–log*p* plot of observed sounding from 0224 UTC 15 Feb at NSSL5. Temperature (°C, solid lines), dewpoint temperature (°C, dashed lines), and winds (one pennant, full barb, and half-barb denote 25, 5, 2.5 m $s^{-1}$, respectively).

the movement of the surface front since the immediate postfrontal cold air was diabatically cooled in a downdraft, as argued in this paper. In contrast, near-surface, postfrontal air from outside this circulation arrived several hours later, as discussed in section 3d. The immediate postfrontal winds were generally too weak to explain the sometimes rapid movement of the front through horizontal advection, so the continual process of convective downdrafts supplying the cold air immediately behind the front, with a component of horizontal advection, all directed by the shortwave trough aloft, must explain the observed cooling and movement of the surface front. Figure 6 shows complicated movements of the front, local accelerations of the front due to convective dynamics [e.g., as discussed by Parker and Johnson (2003b, manuscript submitted to *J. Atmos. Sci.*, hereafter PJb) for their idealized model of a convective line with leading precipitation], and topographic acceleration/retardation of the front, implying the importance of convective-scale and microscale processes in determining frontal movement.

Despite the complicated frontal movement, all surface data support a continuous movement of the front, as opposed to discrete propagation (e.g., Charney and Fritsch 1999; Bryan and Fritsch 2000a,b), despite the presence of the same processes responsible for discrete propagation identified in these studies. The reasons why this event moves continuously rather than discontinuously, however, are beyond the scope of this paper. The results of this study argue that applying simple schemes (e.g., advection by postfrontal winds, gravity current theory) for determining the movement rate of cold fronts on the microscale may not be appropriate.

### *b. Forward tilt*

In a classic rearward-tilting front, subcloud sublimation/evaporation would occur behind the surface position of the front, in the same location as the cold advection behind the front. Indeed, other studies have also discussed the effect of postfrontal evaporation (e.g., Oliver and Holzworth 1953; Garratt 1988; Huang and Emanuel 1991) and sublimation (e.g., Clough and Franks 1991; Barth and Parsons 1996; Parker and Thorpe 1995; Clough et al. 2000) on frontal structure and evolution, showing some similarities to this case, such as the narrow rear-to-front moist downdrafts and the shallowing leading edge to the fronts.

In this event, however, the prefrontal cloud was forward tilting due to the forcing aloft in the presence of the strong vertical wind shear in the environment, as discussed in section 4c. Other studies have shown how strong wind shear can cause forward tilts to cold fronts and/or squall lines (e.g., Parsons 1992; Parker and Johnson 2003a, manuscript submitted to *J. Atmos. Sci.*, hereafter PJa; PJb; PJc), which is also described in other case studies (e.g., Fankhauser et al. 1992; Grady and Verlinde 1997; and others reviewed in section 1a of PJa) and simulated in idealized modeling experiments (e.g., Thorpe et al. 1982; Moncrieff 1989; Lafore and Moncrieff 1989; Shapiro 1992). As a result of this forward tilt to the clouds and precipitation, a greater separation

exists between the cooling due to sublimation/evaporation ahead of the cold front and the cooling due to cold advection behind the cold front.

Such a forward- or downshear-tilting cloud structure is reminiscent of the overturning updraft (e.g., Thorpe et al. 1982) in a ''leading stratiform'' convective system (e.g., Parker and Johnson 2000; PJa; PJb; PJc). We hesitate to use such terminology for this case, however, because, first, stratiform precipitation from the forward-sloping cloud does not reach the surface and, second, this event does not resemble a classic squall line owing to the lack of deep convection and corresponding high radar reflectivity factor.

As we noted, literature addressing the role of postfrontal sublimation or evaporation in frontal structure exists, but literature addressing the role of *prefrontal* sublimation or evaporation on frontal structure is scarce. For example, Crook and Moncrieff (1988) and PJc suggest that cooling due to sublimation below the forward-sloping cloud, which destabilizes the air ahead of the convective line, may intensify such storms and enhance their longevity. In contrast, Parsons (1992) stated, ''creation of the potential instability and the interruption of the inflow by the precipitation [in high-shear situations] creates a [*sic*] unstable flow unlike any airflow observed to date at the leading edge of cold fronts.'' The existence and longevity (western Nevada to northern Utah) of the IPEX IOP 4 cold front and convective line, however, suggest that such systems do exist and provide observational support for the modeling results of Crook and Moncrieff (1988) and PJc.

Forward-tilting fronts were reviewed by Schultz and Steenburgh (1999, sections 1 and 6a). Their review identified two ways by which fronts could become forward tilting: through the interaction of lower-tropospheric and midtropospheric fronts or through the influence of surface friction on the front. This study illustrates a third mechanism—the diabatic cooling caused by sublimating/evaporating hydrometeors from a precipitating cloud aloft.

### *c. Prefrontal trough*

Schultz and Steenburgh (1999) also reviewed prefrontal troughs, or surface pressure troughs that precede the thermal gradient. Sawyer (1946) and Fujita (1959) argued that prefrontal troughs are a result of prefrontal diabatic cooling in other cases. Sanders (1999b) discussed a short-lived front in the southwest United States in which the pressure trough and wind shift separated from the thermal gradient, producing a situation where the deformation was no longer coincident with the thermal gradient, resulting in a weakening of the front. There are some similarities between Sanders' (1999b) event and the event discussed in this paper, namely the increasing distance between the trough and the front (Fig. 9). Nevertheless, in this event, the wind shift stays relatively close to the thermal gradient at each station (Fig. 9), which does not occur in the Sanders (1999b) case. Thus, it would appear that the IPEX IOP 4 front is frontogenetic throughout most of its lifetime, a distinct difference between these two cases.

In IPEX IOP 4, the location of the pressure trough was external to the dynamics of the front itself, unlike what Sanders (1999a) previously argued (where along-front temperature gradients can speed the separation between the trough and thermal gradient). In this case, the location of the pressure trough was due to the onset of the diabatic cooling aloft, which was a function of vertical wind shear and the prefrontal relative humidity profile. With the surface front decelerating in time, greater advection of hydrometeors aloft downstream relative to the front occurred, causing an increasing separation between the prefrontal trough and the surface temperature gradient (e.g., Fig. 9).

Hoxit et al. (1976) and Sun et al. (1993) have shown the existence of upper-level downdrafts on the order of 30–100 km ahead of precipitating systems. Hoxit et al. (1976) have argued that such downdrafts may induce prefrontal troughs. The available datasets from this study are not adequate to assess vertical motion directly, but it is possible that such downdrafts, in concert with the hydrostatic effects of the diabatic cooling, may be responsible for the surface pressure trough, lending further support to our argument that the structure of our front does not conform to simple frontal models.

Such observations indicate that the structure of this cold front was more complicated than simple models of fronts would suggest. The existence of the prefrontal trough excludes this case from behaving like zero- or first-order discontinuity models. More specifically, the zero-order discontinuity defines the front as a discontinuity in temperature (e.g., Bluestein 1993, 240–245), whereas the first-order discontinuity defines the front as a discontinuity in temperature gradient (e.g., Saucier 1955, p. 109; Bluestein 1993, 245–248). In this case, the leading edge of the temperature gradient tilted forward with height, unlike classical models of rearward-tilting fronts. Thus, the nonclassical structure of the cold front was a result of the prefrontal sublimation/evaporation aloft.

## 7. Summary and conceptual model

This paper explores the structure and evolution of a cold front during the Intermountain Precipitation Experiment Intensive Observing Period 4 on 14–15 February 2000. The instrumentation deployed allowed an examination of the microscale structure and evolution of the front as it moved through northern Utah. In particular, subcloud diabatic cooling from a precipitating system aloft played the principal role in the nonclassical frontal structure and evolution during IPEX IOP 4, as the evidence in this paper has demonstrated. This section summarizes the evidence, resulting in a conceptual model for the cold front in this case (Fig. 23).

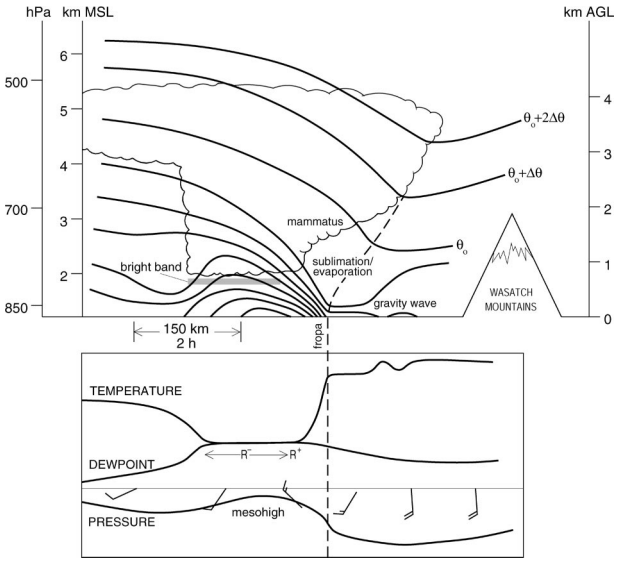


FIG. 23. Conceptual model of the cold front from 14 to 15 Feb 2000. (top) Schematic of cloud (scalloped lines), and potential temperature (thick solid lines). Fropa = surface frontal passage. (bottom) Time series of temperature, dewpoint, sensible weather, winds, and pressure at the surface.

The cold front moved rapidly as it entered northern Utah and decelerated as it moved southward. The rate of surface temperature drop was largest in the north, although the total temperature drop was roughly constant across all of northern Utah. The strong vertical wind shear in the lower troposphere resulted in downshear- or forward-sloping clouds (Fig. 23). From these forward-sloping clouds, snow began to fall, but initially formed mammatus and virga due to the dry subcloud air. In this region, a 20-hPa-deep subcloud superadiabatic layer indicated the cooling by subcloud sublimation. Because of this sublimation, cooling associated with the front started earlier at higher-elevation stations than at lower-elevation stations, although the total temperature drops were largest at low elevations (Fig. 23). Hydrostatically, this cooling aloft resulted in a surface-pressure trough preceding the surface temperature drop. The time between the prefrontal trough and the frontal passage increased as the front decelerated over time.

The forward slope to the clouds also provided another interesting aspect to this case. The surface temperature reached a maximum ahead of the convective line, followed by shading of incoming solar radiation by the forward-sloping cloud, cooling and stabilizing the near-surface air. A solitary gravity wave was manifest at the leading edge of that stable layer (Fig. 10a). After the passage of the wave, the stable layer deepened and the surface temperature dropped several degrees.

Strong and shallow forced lifting occurred at the leading edge of the front. The frontal passage was indicated by the surface temperature dropping abruptly and the dewpoint temperature rising. The coldest postfrontal surface air was consistent with a source region from midlevels as negatively buoyant downdraft air. While being observed by radar, the leading edge of the wind shift line possessed the structure of and evolved like a gravity current (Fig. 20).

Cool, moist air persisted at the surface for several hours after frontal passage. Temperatures rose and dewpoint temperatures dropped as the diabatically cooled air gave way to relatively warmer postfrontal air, possibly associated with a rear-inflow jet (Fig. 23). This recovery was greatest at lower-elevation stations and decreased with height. Aloft, where diabatic cooling did not occur, colder postfrontal air moved into northern Utah associated with the midlevel baroclinic zone on the synoptic scale (e.g., Fig. 3), extending the duration of the temperature drop for higher-elevation stations. The surface mesohigh associated with the cool postfrontal air was associated with northwesterly winds immediately behind the front, followed within 1–2 h by southerly winds (Fig. 23), indicative of the mesohigh and wake-low phenomena associated with mesoscale convective systems.

As a result of the dry subcloud air, the resulting precipitation distribution was a function of elevation with relatively small precipitation amounts near the surface, increasing with height to cloud base. Above cloud base, the majority of stations had nearly the same precipitation amounts, although some stations experienced enhancements or reductions caused by orographic effects.

Although this paper examines just one case, we believe that the results possess some generality. For example, the front associated with IPEX IOP 4 bears some similarities to the front during IOP 7 (Schultz et al. 2002, 203–205), as previously discussed. In addition, other frontal passages in northern Utah show many of the same signatures noted in this paper, suggesting the importance of diabatic cooling in the dry subcloud air to other cases, as well (L. Dunn, J. Shafer, and J. Steenburgh 2003, personal communication).

Because of its dry low-level environment, the Intermountain West would appear to be a favored area for such frontal structures. Similar structures have also been observed in arid regions of China (e.g., Mitsuta et al. 1995; *CFTR* Takemi 1999) and Australia (e.g., Garratt 1998; Ryan et al. 1989; Katzfey and Ryan 1997). It has long been recognized that the classical conceptual models of cyclones and fronts rarely apply to systems in the Intermountain West (e.g., Williams 1972), yet, robust successors have not risen to fill this void. Consequently, without conceptual models of weather systems to draw upon, forecasters have little context within which to place developing weather scenarios and evaluate numerical-model forecast output (e.g., Doswell 1986; Doswell and Maddox 1986; section 2b in Hoffman 1991; Pliske et al. 2003). Hopefully, the analysis of this case, and others in the future from IPEX, will allow development of improved conceptual models of weather systems in the Intermountain West.

*Acknowledgments.* We have benefited considerably from discussions with and comments from Jason Shafer, Fred Sanders, John Horel, Larry Dunn, Ed Zipser, and two anonymous reviewers. Additional assistance and input was provided by Patrick Burke, Dan Cobb, Justin Cox, Jeff Evans, Mark Jackson, David Jorgensen, Jack Kain, Jason Knievel, James LaDue, Paul Neiman, Matthew Parker, James Steenburgh, David Stensrud, and Louis Wicker. William Alder provided the snowfall data and information from *Storm Data*. The Storm Prediction Center graciously provided access to their archives of surface and upper-air maps and data. NCDC provided the 1-minute ASOS data and Grant Goodge helped decode the data. Special thanks go to John Horel, Mike Splitt, Judy Pechmann, and MesoWest for providing radar, profiler, and surface data; David Rust, Sherman Frederickson, and Erik Rasmussen for assistance with the NSSL4 and NSSL5 data; Linda Cheng for providing her quality-controlled precipitation dataset; Joan O'Bannon for her assistance with Fig. 6 and for drafting Fig. 23; and to those individuals and organizations that collected data or facilitated data collection during IPEX. Thanks also to the governmental agencies, commercial firms, and educational institutions that provide data to MesoWest and make this type of research possible. Much of the research on this case was performed during fall 2002 while Schultz was visiting the Department of Meteorology at the University of Utah; their support is gratefully acknowledged. Funding was provided by NOAA/OAR/NSSL under NOAA–OU Cooperative Agreement #NA17RJ1227.

## REFERENCES

Barnes, S. L., 1964: A technique for maximizing details in numerical weather map analysis. *J. Appl. Meteor.*, **3,** 396–409.

Barth, M. C., and D. B. Parsons, 1996: Microphysical processes associated with intense frontal rainbands and the effect of evaporation and melting on frontal dynamics. *J. Atmos. Sci.*, **53,** 1569–1586.

Benjamin, S. G., J. M. Brown, K. J. Brundage, B. Schwartz, T. Smirnova, T. L. Smith, L. L. Morone, and G. J. DiMego, 1998: The operational RUC-2. Preprints, *16th Conf. on Weather Analysis and Forecasting*, Phoenix, AZ, Amer. Meteor. Soc., 249–252.

Berson, F. A., 1958: Some measurements on undercutting cold air. *Quart. J. Roy. Meteor. Soc.*, **84,** 1–16.

Bjerknes, J., 1919: On the structure of moving cyclones. *Geophys. Publ.*, **1** (2), 1–8.

Bluestein, H. B., 1993: *Observations and Theory of Weather Systems.* Vol. 2, *Synoptic–Dynamic Meteorology in Midlatitudes*, Oxford University Press, 594 pp.

Braun, S. A., R. Rotunno, and J. B. Klemp, 1999: Effects of coastal orography on landfalling cold fronts. Part I: Dry, inviscid dynamics. *J. Atmos. Sci.*, **56,** 517–533.

Browning, K. A., 1990: Organization of clouds and precipitation in extratropical cyclones. *Extratropical Cyclones*: *The Erik Palmén Memorial Volume*, C. W. Newton and E. O. Holopainen, Eds., Amer. Meteor. Soc., 129–153.

——, and T. W. Harrold, 1970: Air motion and precipitation growth at a cold front. *Quart. J. Roy. Meteor. Soc.*, **96,** 369–389.

Brundidge, K. C., 1965: The wind and temperature structure of nocturnal cold fronts in the first 1,420 feet. *Mon. Wea. Rev.*, **93,** 587–603.

Bryan, G. H., and J. M. Fritsch, 2000a: Discrete propagation of surface fronts in a convective environment: Observations and theory. *J. Atmos. Sci.*, **57,** 2041–2060.

——, and ——, 2000b: Diabatically driven discrete propagation of surface fronts: A numerical analysis. *J. Atmos. Sci.*, **57,** 2061–2079.

Carbone, R. E., 1982: A severe frontal rainband. Part I: Stormwide hydrodynamic structure. *J. Atmos. Sci.*, **39,** 258–279.

Charney, J. J., and J. M. Fritsch, 1999: Discrete frontal propagation in a nonconvective environment. *Mon. Wea. Rev.*, **127,** 2083–2101.

Cheng, L., 2001: Validation of quantitative precipitation forecasts during the Intermountain Precipitation Experiment. M.S. thesis, Dept. of Meteorology, University of Utah, 137 pp. [Available online at http://www.met.utah.edu/jhorel/homepages/lcheng/thesis.html.]

Clough, S. A., and R. A. A. Franks, 1991: The evaporation of frontal and other stratiform precipitation. *Quart. J. Roy. Meteor. Soc.*, **117,** 1057–1080.

——, H. W. Lean, N. M. Roberts, and R. M. Forbes, 2000: Dynamical effects of ice sublimation in a frontal wave. *Quart. J. Roy. Meteor. Soc.*, **126,** 2405–2434.

Colle, B. A., B. F. Smull, and M.-J. Yang, 2002: Numerical simulations of a landfalling cold front observed during COAST: Rapid evolution and responsible mechanisms. *Mon. Wea. Rev.*, **130,** 1945–1966.

Cox, J. A. W., 2002: Kinematic structure of a Wasatch Mountain snowstorm. M.S. thesis, Dept. of Meteorology, University of Utah, 60 pp. [Available online at http://www.met.utah.edu/jimsteen/theses/cox02_thesis.pdf.]

Crook, N. A., and M. W. Moncrieff, 1988: The effect of large-scale convergence on the generation and maintenance of deep moist convection. *J. Atmos. Sci.*, **45,** 3606–3624.

Dickinson, M. J., and D. J. Knight, 1999: Frontal interaction with mesoscale topography. *J. Atmos. Sci.*, **56,** 3544–3559.

Doesken, N. J., and G. L. Schaefer, 1987: The contribution of SNOTEL precipitation measurements to climate analysis, monitoring and research in Colorado. *Proc. Western Snow Conf., 55th Annual Meeting*, Vancouver, BC, Canada, Western Snow Conference, 20–30.

Doswell, C. A., III, 1986: The human element in weather forecasting. *Natl. Wea. Dig.*, **11** (2), 6–17.

——, and R. A. Maddox, 1986: The role of diagnosis in weather forecasting. Preprints, *11th Conf. on Weather Forecasting and Analysis*, Kansas City, MO, Amer. Meteor. Soc., 177–182.

——, and E. N. Rasmussen, 1994: The effect of neglecting the virtual temperature correction on CAPE calculations. *Wea. Forecasting*, **9,** 625–629.

Dunn, L. B., 1983: Quantitative and spacial [*sic*] distribution of winter precipitation along Utah's Wasatch Front. NOAA Tech. Memo. NWS WR-181, 72 pp. [Available from NOAA NWS Western Region Headquarters, 125 S. State Street, Rm. 1311, Salt Lake City, UT 84138-1102.]

Emanuel, K. A., 1994: *Atmospheric Convection.* Oxford University Press, 580 pp.

Fankhauser, J. C., G. M. Barnes, and M. A. LeMone, 1992: Structure of a midlatitude squall line formed in strong unidirectional shear. *Mon. Wea. Rev.*, **120,** 237–260.

Fujita, T., 1959: Precipitation and cold air production in mesoscale thunderstorm systems. *J. Meteor.*, **16,** 454–466.

Gallus, W. A., Jr., and M. Segal, 1999: Cold front acceleration over Lake Michigan. *Wea. Forecasting*, **14,** 771–781.

Garratt, J. R., 1988: Summertime cold fronts in southeast Australia—Behavior and low-level structure of main frontal types. *Mon. Wea. Rev.*, **116,** 636–649.

Gaudet, B., and W. R. Cotton, 1998: Statistical characteristics of a real-time precipitation forecasting model. *Wea. Forecasting*, **13,** 966–982.

Gilmore, M. S., and L. J. Wicker, 1998: The influence of midtro-

pospheric dryness on supercell morphology and evolution. *Mon. Wea. Rev.*, **126,** 943–958.
Grady, R. L., and J. Verlinde, 1997: Triple-Doppler analysis of a discretely propagating, long-lived, High Plains squall line. *J. Atmos. Sci.,* **54,** 2729–2748.
Hanstrum, B. N., G. A. Mills, A. Watson, J. P. Monteverdi, and C. A. Doswell III, 2002: The cool-season tornadoes of California and southern Australia. *Wea. Forecasting,* **17,** 705–722.
Hobbs, P. V., and P. O. G. Persson, 1982: The mesoscale and microscale structure and organization of clouds and precipitation in midlatitude cyclones. Part V: The substructure of narrow cold-frontal rainbands. *J. Atmos. Sci.,* **39,** 280–295.
Hoffman, R. R., 1991: Human factors psychology in the support of forecasting: The design of advanced meteorological workstations. *Wea. Forecasting,* **6,** 98–110.
Horel, J., and Coauthors, 2002: MesoWest: Cooperative mesonets in the western United States. *Bull. Amer. Meteor. Soc.,* **83,** 211–225.
Houze, R. A., Jr., 1997: Stratiform precipitation in regions of convection: A meteorological paradox? *Bull. Amer. Meteor. Soc.*, **78,** 2179–2196.
Hoxit, L. R., C. F. Chappell, and J. M. Fritsch, 1976: Formation of mesolows or pressure troughs in advance of cumulonimbus clouds. *Mon. Wea. Rev.,* **104,** 1419–1428.
Huang, H.-C., and K. A. Emanuel, 1991: The effects of evaporation on frontal circulations. *J. Atmos. Sci.,* **48,** 619–628.
Johns, R. H., J. M. Davies, and P. W. Leftwich, 1993: Some wind and instability parameters associated with strong and violent tornadoes. 2. Variations in the combinations of wind and instability parameters. *The Tornado: Its Structure, Dynamics, Prediction, and Hazards, Geophys. Monogr.*, No. 79, Amer. Geophys. Union, 583–590.
Johnson, R. H., 2001: Surface mesohighs and mesolows. *Bull. Amer. Meteor. Soc.*, **82,** 13–31.
Katzfey, J. J., and B. F. Ryan, 1997: Modification of the thermodynamic structure of the lower troposphere by the evaporation of precipitation: A GEWEX cloud system study. *Mon. Wea. Rev.*, **125,** 1431–1446.
Keyser, D., 1986: Atmospheric fronts: An observational perspective. *Mesoscale Meteorology and Forecasting,* P. S. Ray, Ed., Amer. Meteor. Soc., 216–258.
Knievel, J. C., 2001: The kinematics and thermodynamics of a midlatitude, continental mesoscale convective system and its mesoscale vortex. Ph.D. dissertation, Colorado State University, 99 pp. [Available from the Dept. of Atmospheric Science, Colorado State University, Fort Collins, CO 80523-1371.]
LaDue, J. G., 2002: The structure of a tornadic bow echo in Idaho. Preprints, *21st Conf. on Severe Local Storms,* San Antonio, TX, Amer. Meteor. Soc., 490–493.
Lafore, J.-P., and M. W. Moncrieff, 1989: A numerical investigation of the organization and interaction of the convective and stratiform regions of tropical squall lines. *J. Atmos. Sci.,* **46,** 521–544.
Locatelli, J. D., M. T. Stoelinga, and P. V. Hobbs, 1998: Structure and evolution of winter cyclones in the central United States and their effects on the distribution of precipitation. Part V: Thermodynamic and dual-Doppler radar analysis of a squall line associated with a cold front aloft. *Mon. Wea. Rev.,* **126,** 860–875.
McMillan, G. D., 1981: SNOTEL: A management tool for the future. *Proc. 49th Western Snow Conf.*, St. George, UT, Western Snow Conference, 116–119.
Mitsuta, Y., T. Hayashi, T. Takemi, Y. Hu, J. Wang, and M. Chen, 1995: Two severe local storms as observed in the arid area of northwest China. *J. Meteor. Soc. Japan,* **73,** 1269–1284.
Moller, A. R., 2001: Severe local storms forecasting. *Severe Convective Storms, Meteor. Monogr.*, No. 50, Amer. Meteor. Soc., 433–480.
Moncrieff, M. W., 1989: Analytical models of narrow cold-frontal rainbands and related phenomena. *J. Atmos. Sci.,* **46,** 150–162.
NCDC, 2000: *Storm Data.* Vol. 42, No. 2, 127 pp.
Oliver, V. J., and G. C. Holzworth, 1953: Some effects of the evaporation of widespread precipitation on the production of fronts and on changes in frontal slopes and motion. *Mon. Wea. Rev.,* **81,** 141–151.
Parker, D. J., and A. J. Thorpe, 1995: The role of snow sublimation in frontogenesis. *Quart. J. Roy. Meteor. Soc.,* **121,** 763–782.
Parker, M. D., and R. H. Johnson, 2000: Organizational modes of midlatitude mesoscale convective systems. *Mon. Wea. Rev.,* **128,** 3413–3436.
——, and ——, 2003a: Structure and dynamics of quasi-2D mesoscale convective systems. *J. Atmos. Sci.,* submitted.
——, and ——, 2003b: Simulated convective lines with leading precipitation. Part I: Governing dynamics. *J. Atmos. Sci.,* submitted.
——, and ——, 2003c: Simulated convective lines with leading precipitation. Part II: Evolution and maintenance. *J. Atmos. Sci.,* submitted.
Parsons, D. B., 1992: An explanation for intense frontal updrafts and narrow cold-frontal rainbands. *J. Atmos. Sci.,* **49,** 1810–1825.
Pliske, R., B. Crandall, and G. Klein, 2003: Competence in weather forecasting. *Psychological Investigations of Competent Decision Making,* J. Shanteau et al., Eds., Cambridge University Press, in press.
Rust, W. D., R. Davies-Jones, D. W. Burgess, R. A. Maddox, L. C. Showell, T. C. Marshall, and D. K. Lauritsen, 1990: Testing a mobile version of a Cross-chain Loran Atmospheric Sounding System (M-CLASS). *Bull. Amer. Meteor. Soc.,* **71,** 173–180.
Ryan, B. F., K. J. Wilson, and E. J. Zipser, 1989: Modification of the thermodynamic structure of the lower troposphere by the evaporation of precipitation ahead of a cold front. *Mon. Wea. Rev.,* **117,** 138–153.
Sanders, F., 1999a: A proposed method of surface map analysis. *Mon. Wea. Rev.,* **127,** 945–955.
——, 1999b: A short-lived cold front in the southwestern United States. *Mon. Wea. Rev.,* **127,** 2395–2403.
——, and C. A. Doswell III, 1995: A case for detailed surface analysis. *Bull. Amer. Meteor. Soc.,* **76,** 505–521.
Saucier, W. J., 1955: *Principles of Meteorological Analysis.* The University of Chicago Press, 438 pp.
Sawyer, J. S., 1946: Cooling by rain as a cause of the pressure rise in convectional squalls. *Quart. J. Roy. Meteor. Soc.,* **72,** 168.
Schultz, D. M., and W. J. Steenburgh, 1999: The formation of a forward-tilting cold front with multiple cloud bands during Superstorm 1993. *Mon. Wea. Rev.,* **127,** 1108–1124.
——, and Coauthors, 2002: Understanding Utah winter storms: The Intermountain Precipitation Experiment. *Bull. Amer. Meteor. Soc.,* **83,** 189–210.
Schumacher, P. N., D. J. Knight, and L. F. Bosart, 1996: Frontal interaction with the Appalachian Mountains. Part I: A climatology. *Mon. Wea. Rev.,* **124,** 2453–2468.
Shapiro, A., 1992: A hydrodynamical model of shear flow over semi-infinite barriers with application to density currents. *J. Atmos. Sci.,* **49,** 2293–2305.
Shapiro, M. A., 1984: Meteorological tower measurements of a surface cold front. *Mon. Wea. Rev.,* **112,** 1634–1639.
Simpson, J. E., 1997: *Gravity Currents in the Environment and the Laboratory.* 2d ed. Cambridge University Press, 244 pp.
Smith, R. K., and M. J. Reeder, 1988: On the movement and low-level structure of cold fronts. *Mon. Wea. Rev.,* **116,** 1927–1944.
Steenburgh, W. J., 2003: One hundred inches in one hundred hours—Evolution of a Wasatch Mountain winter storm cycle. *Wea. Forecasting,* in press.
——, and T. R. Blazek, 2001: Topographic distortion of a cold front over the Snake River Plain and central Idaho mountains. *Wea. Forecasting,* **16,** 301–314.
Stensrud, D. J., R. A. Maddox, and C. L. Ziegler, 1991: A sublimation-initiated mesoscale downdraft and its relation to the wind field below a precipitating anvil cloud. *Mon. Wea. Rev.,* **119,** 2124–2139.
Stumpf, G. J., R. H. Johnson, and B. F. Small, 1991: The wake low

in a midlatitude mesoscale convective system having complex convective organization. *Mon. Wea. Rev.*, **119,** 134–158.

Sun, J., S. Braun, M. I. Biggerstaff, R. G. Fovell, and R. A. Houze Jr., 1993: Warm upper-level downdrafts associated with a squall line. *Mon. Wea. Rev.*, **121,** 2919–2927.

Takemi, T., 1999: Structure and evolution of a severe squall line over the arid region in northwest China. *Mon. Wea. Rev.*, **127,** 1301–1309.

Thorpe, A. J., M. J. Miller, and M. W. Moncrieff, 1982: Two-dimensional convection in non-constant shear: A model of mid-latitude squall lines. *Quart. J. Roy. Meteor. Soc.*, **108,** 739–762.

Tory, K. J., and M. J. Reeder, 1996: A numerical study of the influence of a diurnally forced planetary boundary-layer on dry frontogenesis. Preprints, *Seventh Conf. on Mesoscale Processes*, Reading, United Kingdom, Amer. Meteor. Soc., 517–519.

Trapp, R. J., and C. A. Doswell III, 2000: Radar data objective analysis. *J. Atmos. Oceanic Technol.*, **17,** 105–120.

Weisman, M. L., J. B. Klemp, and R. Rotunno, 1988: Structure and evolution of numerically simulated squall lines. *J. Atmos. Sci.*, **45,** 1990–2013.

Williams, P., Jr., 1972: Western Region synoptic analysis—Problems and methods. NOAA NWS Western Region Tech. Memo. NWSTM WR-71, 71 pp. [Available from NOAA NWS Western Region Headquarters, 125 S. State Street, Rm. 1311, Salt Lake City, UT 84138-1102.]

——, and E. L. Peck, 1962: Terrain influences on precipitation in the Intermountain West as related to synoptic situations. *J. Appl. Meteor.*, **1,** 343–347.

Williams, S. F., C. G. Wade, and C. Morel, 1993: A comparison of high resolution radiosonde winds: 6-second Micro-ART winds versus 10-second CLASS Loran winds. Preprints, *Eighth Symp. on Meteorological Observations and Instrumentation*, Anaheim, CA, Amer. Meteor. Soc., 60–65.

Wurman, J., J. Straka, E. Rasmussen, M. Randall, and A. Zahrai, 1997: Design and deployment of a portable, pencil-beam, pulsed, 3-cm Doppler radar. *J. Atmos. Oceanic Technol.*, **14,** 1502–1512.

Zehnder, J. A., and P. R. Bannon, 1988: Frontogenesis over a mountain ridge. *J. Atmos. Sci.*, **45,** 628–644.

Zipser, E. J., 1969: The role of organized unsaturated convective downdrafts in the structure and rapid decay of an equatorial disturbance. *J. Appl. Meteor.*, **8,** 799–814.

——, 1977: Mesoscale and convective-scale downdrafts as distinct components of squall-line structure. *Mon. Wea. Rev.*, **105,** 1568–1589.